

We are IntechOpen, the world's leading publisher of Open Access books Built by scientists, for scientists

6,900

Open access books available

185,000

International authors and editors

200M

Downloads

Our authors are among the

154

Countries delivered to

TOP 1%

most cited scientists

12.2%

Contributors from top 500 universities



WEB OF SCIENCE™

Selection of our books indexed in the Book Citation Index
in Web of Science™ Core Collection (BKCI)

Interested in publishing with us?
Contact book.department@intechopen.com

Numbers displayed above are based on latest data collected.
For more information visit www.intechopen.com



Applications of Al Modified Graphene on Gas Sensors and Hydrogen Storage

Zhimin Ao, Jack Yang and Sean Li
*School of Materials Science and Engineering,
The University of New South Wales, NSW 2052
Australia*

1. Introduction

Graphene is a single layer of graphite with a hexagonal structure, or an individual sheet of sp^2 -hybridized carbon bound in two dimensions. It was experimentally fabricated for the first time through mechanical exfoliation of small mesas from highly oriented pyrolytic graphite (HOPG) in 2004 and subsequently was found with excellent electrical properties (Novoselov et al., 2004). This discovery has triggered enormous amount of interest on graphene both in fundamental and applied research. Graphene has shown promising applications as ultra-sensitive gas sensors, transparent electrodes in liquid crystal display devices, and large capacity electrodes in Li batteries (Rao et al., 2009).

Various methods have been reported for the synthesis of single-layer graphene: (1) Mechanical exfoliation from HOPG (Novoselov et al., 2004; Zhang et al., 2005), which is deposited on to a silicon substrate. This method is low cost, but the graphene produced is of poor quality with the limited area. It is particularly difficult and time-consuming to synthesize single-layer graphene in large scale with this method (Yuan et al., 2009). (2) Chemical exfoliation from bulk graphite (Li et al., 2008a;b). In this case, oxidized graphite (by using strong acids) was cleaved via rapid thermal expansion or ultrasonic dispersion, and subsequently the graphene oxide sheets were reduced to graphene. A serious drawback of this method is that the oxidation process induces a variety of defects which would degrade the electronic properties of graphene. (3) Epitaxial growth on an insulator surface (such as SiC) (Zhou et al., 2007). The graphene obtained showed poor uniformity and contained a multitude of domains. (4) Chemical vapour deposition (CVD) on the surfaces of metals (e.g., Ni) (Reina et al., 2009). Recently, N substitutionally doped graphene was first synthesized by a CVD method with the presence of CH_4 and NH_3 (Wei et al., 2009). As doping accompanies with the recombination of carbon atoms into graphene in the CVD process, dopant atoms can be substitutionally doped into the graphene lattice, which is hard to realize by other synthetic methods.

Several unique electronic properties associated with these 2D crystals have been discovered (Beenakker, 2008). In addition, it is known that carbon nanotubes have good sensor properties (Geim & Novoselov, 2007). Recently, graphenes as highly sensitive gas sensors were also reported (Ao et al., 2008; Bunch et al., 2005; Yang et al., 2010). It was shown that the increase in graphene charge carrier concentration induced by adsorbed gas molecules could be utilized to make highly sensitive sensors, even with the possibility of detecting individual molecules. The sensing property is based on the changes in the resistivity due to molecules adsorbed on

graphene sheet that act as donors or acceptors. The sensitivity of NH_3 , CO , and H_2O up to 1 ppb (parts per 10^9) was demonstrated, and even the ultimate sensitivity of an individual molecule was suggested for NO_2 . Furthermore, the preliminary works (Ao et al., 2009a) indicated that graphene have promising physisorption properties for hydrogen.

With state-of-art computer simulations, it is believed that the properties of condensed matters can be understood at the atomic level. In the simulation, the simulator builds a model of a real system and explores its properties. In many ways, simulation studies share the same mentality as experimental ones. However, simulations allow absolute control over the experimental parameters and access to the outcomes in details. These strengths have been exploited for the last fifty years since the introduction of computation algorithms that allows one to calculate the properties of materials based on the first-principles in light of fundamental physics outlined in Schrödinger equation without free parameters. In this chapter, the applications of Al modified graphene as gas sensor and hydrogen storage materials are developed and optimized with density functional theories (DFT).

2. Application for ultra-sensitive carbon oxide detection

2.1 Emerging ultra-high sensitive CO detection

It was reported that the detectable range and sensitivity of the single wall carbon nanotubes (SWCNTs) can be widened and enhanced substantially through either doping technology or surface engineering (Kong et al., 2001; Peng & Cho, 2003; Wei et al., 2004). For example, SWCNT coated with Pb nanoparticles has high sensitivity to H_2 (Kong et al., 2001), SnO_2 /SWCNTs hybrid material shows an enhanced sensitivity to NO_2 (Wei et al., 2004). The high sensitivity of boron doped SWCNT to CO and H_2O absorptions has been also demonstrated (Peng & Cho, 2003). Most recently, Al-cluster and Al doped SWCNT assembly were suggested to be promising systems for novel molecular sensors to NH_3 (Zhao et al., 2005) and CO (Wang et al., 2007), and the B doped SWCNTs are highly sensitive to the gaseous cyanide and formaldehyde molecules (Zhang et al., 2006). However, the devices with higher sensitivity to these toxic gases are apparently required for environmental safety issues both in workplaces and residential areas, especially in some industrial and military fields.

Graphene based device may be a solution for ultra-high sensitivity gas sensor (Leenaerts et al., 2008; Schedin et al., 2007; Wehling et al., 2008). Similar to CNT, the working principle of graphene devices as gas sensors is based on the changes of their electrical conductivity induced by surface adsorbates, which act as either donors or acceptors associated with their chemical natures and preferential adsorption sites (Collins et al., 2000; Kong et al., 2000; Moseley, 1997). Graphene is considered to be an excellent sensor material and the sensitivity of Al doped graphene system to CO gas detection is investigated using DFT calculations.

2.2 Rationale for choosing Al as candidate dopant: a quantum field theoretical perspective

Since graphene is a stable 2D structure, gas molecules tend to be adsorbed onto pristine graphene weakly through physisorption. This has brought a large disadvantage for using pristine graphene to adsorb toxic gases such as CO . By introducing substituent impurities into graphene through chemical doping, the local electronic structures around the dopants could be modified. Typically, as confirmed by the first principle studies in the next section, incorporating Al into graphene will cause a distortion to the electron density distribution around the dopant. In this case, C-atoms surrounding the Al dopant will attract electrons due to their high electron affinity, whereas on the Al dopant, a decrease in electron density can be observed. The charge redistribution makes the Al to be an active site for CO adsorption. This

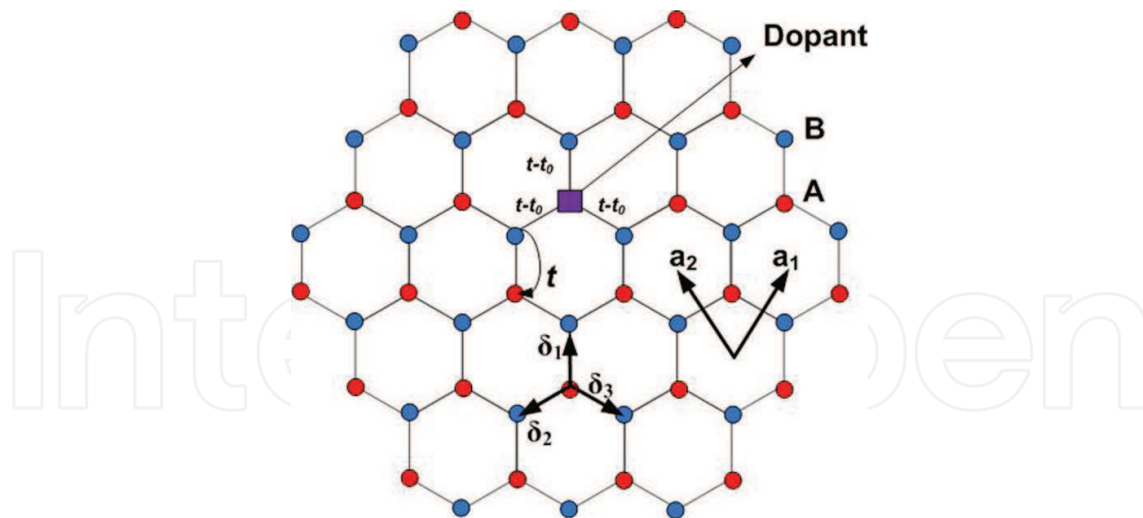


Fig. 1. The honeycomb graphene lattice with a substituting atom replacing a carbon atom. The substituent changes the local hopping parameter from t to $t - t_0$. The honeycomb lattice is considered as made up with two sublattices with atomic types A and B. In this case, an A-type atom has been substituted with an impurity atom.

charge re-distribution effect can be confirmed with advanced field theoretical methods (Peres et al., 2006; 2007; 2009).

Here, the electronic properties caused by a single dopant in graphene layer can also be studied with the field theory.

Under the tight-binding model, the graphene honeycomb lattice can be considered as being constructed from unit cells consisting two types of atoms A and B (Fig. 1). The unit cell vectors in Cartesian coordinates are $\vec{a}_1 = \frac{a_0}{2}(3, \sqrt{3})$ and $\vec{a}_2 = \frac{a_0}{2}(3, -\sqrt{3})$, with a_0 to be the unit cell parameter. $\vec{\delta}_n$ ($n = 1, 2, 3$) are vectors connecting a given atom to its three direct neighbours. Introducing a phase factor $\varphi(k) = \sum_{i=1}^3 e^{ik\delta_i}$, the tight-binding Hamiltonian for graphene, with a single impurity substituting an A-type atom, can be expressed as

$$\hat{\mathcal{H}} = -t \sum_{k,\sigma} \left(\varphi(k) \hat{a}_{k,\sigma}^\dagger \hat{b}_{k,\sigma} + h.c. \right) + \frac{t_0}{N_c} \sum_{k,k',\sigma} \left(\varphi(k') \hat{a}_{k,\sigma}^\dagger \hat{b}_{k',\sigma} + h.c. \right) + \sum_k \frac{\varepsilon_0}{N_c} \hat{a}_{k,\sigma}^\dagger \hat{a}_{k,\sigma}, \quad (1)$$

in the reciprocal space. In the above Hamiltonian, $\hat{a}_{k,\sigma}^\dagger$ ($\hat{b}_{k,\sigma}^\dagger$) and $\hat{a}_{k,\sigma}$ ($\hat{b}_{k,\sigma}$) creates and destroys an electron with wavevector k and spin on A(B) lattice site, respectively. N_c is the number of atoms in a unit cell. The spin degree of freedom is summed over spin index σ . The hopping parameter between two neighboring C atoms is t , where upon dopant substitution, the hopping parameters between the dopant and its neighboring C atoms are changed to $t - t_0$. The dopant atom also introduces a local potential ε_0 . By changing the impurity hopping parameters and local potential, different impurity types can be modeled, which will become apparent later.

Our aim is to calculate the electronic density of states (DOS) on the impurity and its nearest neighboring sites. This requires the knowledge of the system's Green's function. Under the Matsubara formalism, it reads

$$G_\sigma(\omega_n, k, p) = \begin{pmatrix} G_{aa}(\omega_n, k, p) & G_{ab}(\omega_n, k, p) \\ G_{ba}(\omega_n, k, p) & G_{bb}(\omega_n, k, p) \end{pmatrix}, \quad (2)$$

in which the matrix elements $G_{\alpha\beta}(\omega_n, k, p)$ are defined as the Fourier transforms of $G_{\alpha\beta}(k, p, \tau) = -\langle T_\tau [\hat{\alpha}_k^\dagger(\tau)\hat{\beta}_p(0)] \rangle$ with $\alpha, \beta = a, b$. k and p denotes the electronic wavevectors τ is the complex time variable and ω_n are the fermionic Matsubara frequencies.

The system Green's function (Eq. 2) can be solved from the equations-of-motion derived based on Hamiltonian (Eq. 1). The rationale behind the solution procedure is to seek for the relationship behind $G_\sigma(\omega_n, k, p)$ and $G_\sigma^0(\omega_n, k)$. the Matsubara Green's function for pristine graphene, where the later can be expressed analytically as (Peres et al., 2006):

$$G_\sigma^0(\omega_n, k) = \begin{pmatrix} G_{aa}^0(\omega_n, k) & G_{ab}^0(\omega_n, k) \\ G_{ba}^0(\omega_n, k) & G_{bb}^0(\omega_n, k) \end{pmatrix} = \sum_{j=\pm 1} \frac{1/2}{i\omega_n - j|\varphi(k)|} \begin{pmatrix} 1 & je^{i\delta(k)} \\ je^{-i\delta(k)} & 1 \end{pmatrix}, \quad (3)$$

with $e^{i\delta(k)} = \varphi(k)/|\varphi(k)|$.

Since we are interested in the electronic DOS on the impurity (A) site and its nearest-neighboring (B) sites, therefore, it would be sufficient to solve for $G_{aa}(\omega_n, k, p)$ and $G_{bb}(\omega_n, k, p)$ in Eq. 2. The electronic DOS can then be found from the imaginary parts of the retarded Green's functions $G_{aa}^r(\omega, k, p)$ and $G_{bb}^r(\omega, k, p)$ through analytical continuation of the Matsubara Green's functions. The presence of both diagonal and nondiagonal disorders means that the solutions will be of a more complex form than the usual T -matrix for a single Anderson impurity scattering problem, and the results are

$$G_{aa}(\omega_n, k, p) = \delta_{k,p}G_{aa}^0(\omega_n, k) + g(\omega_n) + h(\omega_n) \left[G_{aa}^0(\omega_n, k) + G_{aa}^0(\omega, p) \right] + G_{aa}(\omega_n, k)T(\omega_n)G_{aa}^0(\omega_n, p), \quad (4)$$

$$G_{bb}(\omega_n, k, p) = \delta_{k,p}G_{bb}^0(\omega_n, k) + \frac{t^2\varphi^*(k)\varphi(p)}{(i\omega)^2}G_{bb}^0(\omega_n, k)T(\omega_n)G_{bb}^0(\omega_n, p), \quad (5)$$

where

$$g(\omega_n) = t_0^2\bar{G}_{aa}^0(\omega_n)/[N_cD(\omega_n)], \quad (6)$$

$$h(\omega_n) = t_0(t - t_0)/[N_cD(\omega_0)], \quad (7)$$

and

$$T(\omega_n) = -[i\omega_n t_0(2t - t_0) - \varepsilon_0 t^2]/[N_cD(\omega_n)], \quad (8)$$

with

$$D(\omega_n) = (t - t_0)^2 + [i\omega_n t_0(t - t_0) - \varepsilon_0 t^2] \bar{G}_{aa}^0(\omega_n), \quad (9)$$

and

$$\bar{G}_{aa}^0(\omega_n) = \frac{1}{N_c} \sum_k G_{aa}^0(\omega_n, k). \quad (10)$$

The important term is the $g(\omega_n)$ whose double Fourier transform gives $G_{aa}(\omega_n, 0, 0)$ which is the return (back-scattering) amplitude of the electron wave to the impurity site. Its magnitude, which depends on $D(\omega_n)$, depicts the electronic DOS on the impurity sites.

In the case of Al doping, where the dopant has a larger atomic radius than carbon, we can let $t_0 = -t$, with $\varepsilon_0 < 0$, as a limiting case. This gives,

$$g_1(\omega_n) = \frac{\bar{G}^0(\omega_n)}{(4 - 4i\omega_n\bar{G}^0(\omega_n)) + (i\omega_n - \varepsilon_0\bar{G}^0(\omega_n))}. \quad (11)$$

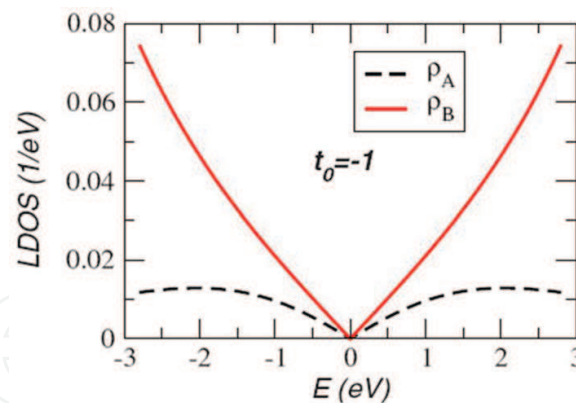


Fig. 2. Local density of states (LDOS) on the impurity atom at A site and surrounding carbon atoms at B sites for the case where $t_0 = -1$, $t = 1$, mimicking the situation of Al doping in graphene. (Reproduced with permission from Ref. (Peres et al., 2009). Copyright 2009, APS)

On the other hand, for a dopant with smaller ionic radius, we would have $\varepsilon_0 > 0$ and $t_0 = |\gamma|t$. The most interesting case is for a physisorbed species on graphene layer, in which $t_0 = t$, indicating that the molecule would have no interaction with the graphene layer. Under such a condition, the Matsubara Green's function for a free particle can be reclaimed as,

$$g_2(\omega_n) = \frac{1}{i\omega_n - \varepsilon_0}. \quad (12)$$

Fig. 2 shows the resulting electronic DOS on the impurity site and its neighboring carbon atoms with $t_0 = -t$. In this case, the ε_0 is chosen to be zero, whereas a nonzero ε_0 will simply modify the DOS diagram by destroying the particle-hole symmetry. It is hence evident from Fig. 2 that effect of an Al-like dopant is to deplete electrons from the impurity and causing electron accumulation in the surrounding atoms ($\rho_A < \rho_B$).

2.3 CO adsorption effects on atomic configuration, electronic energy and bond lengths of Al doped graphene

Above analysis established a solid theoretical framework for further investigation of the Al doped graphene for application of CO sensor with DFT calculations. In this work, all DFT calculations were performed in Dmol³ code (Delley, 1990). It is widely known that calculations limited at the local density approximation (LDA) overestimate bond energy E_b and underestimate equilibrium distances (Jeloaica & Sidis, 1999; Lugo-Solis & Vasiliev, 2007). Thus, a GGA with the RPBE method is used as the exchange correlation function (Hammer et al., 1999). The DFT semicore pseudopotential (DSPP) core treatment (Delley, 2002) was implemented for relativistic effects, which replaces core electrons by a single effective potential. To ensure that the results of the calculations were comparable, identical conditions had been employed for the isolated CO molecule, the original Al doped graphene and also the adsorbed graphene system. The k -point was set to $6 \times 6 \times 2$ for all slabs, which brought out the convergence tolerance of energy of 1.0×10^{-5} hartree (1 hartree = 27.21 eV), and that of maximum force of 0.002 hartree.

In the simulation, three-dimensional periodic boundary condition had been adopted and C-O bond length was set to $l_{C-O} = 1.13 \text{ \AA}$, which is consistent with experimental results (Lide, 2000). For the graphene, a single layer 2×2 supercell with a vacuum width of 12 Å above had been constructed, which ensured that the interaction between repeated slabs in a direction

normal to the surface was small enough. All atoms were allowed to relax for all energy calculations. The adsorption energy E_b between the CO gas molecule and graphene is defined as,

$$E_b = E_{\text{CO+graphene}} - (E_{\text{graphene}} + E_{\text{CO}}), \quad (13)$$

where the subscripts CO+graphene, graphene, and CO denote the adsorbed system, isolated graphene and CO molecules, respectively.

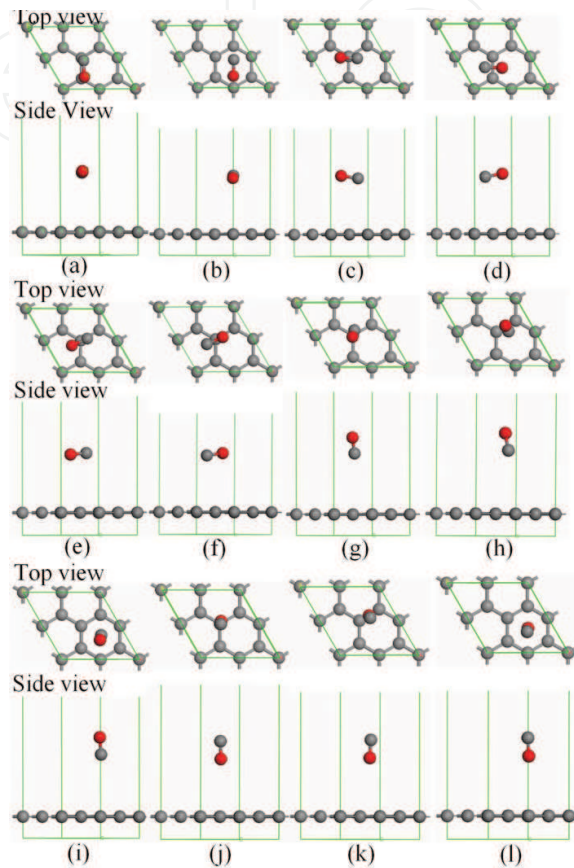


Fig. 3. Twelve available binding sites for CO adsorbed on intrinsic graphene (top and below images show the top and side view, respectively). (a) T-B-T, (b) T-H-T, (c) H-T-H, (d) H-B-H, (e) B(C atom)-T-H, (f) B(O atom)-T-H, (g) T(O atom upward), (h) B(O atom upward), (i) H(O atom upward), (j) T(C atom upward), (k) B(C atom upward), (l) H(C atom upward). T, B and H denote top site of C atoms, bridge site of C-C bond and hollow site of carbon hexagon, respectively. Gray, pink and red spheres are denoted as C, Al and O atoms, respectively. (Reproduced with permission from Ref. (Ao et al., 2008). Copyright 2008, Elsevier)

To search for the most stable structure between a CO molecule and the intrinsic graphene, E_b described in Eq. 13 and the binding distance, d , for all possible configurations were calculated. Twelve possible binding sites for the CO adsorbed on graphene layer were considered as initial structures as shown in Fig. 3(a)-(l). After full structural relaxation, no distinctive structural change has been found. All of the results are displayed in Table 1. It is found that adsorption configuration shown in Fig. 3(f) has the smallest d value and the largest E_b value among all the possible configurations. This indicates that the configuration shown in Fig. 3(f) is the most stable atomic arrangement with the strongest interaction between CO and graphene with $E_b = 0.016$ eV and $d = 3.768$ Å, which are consistent with the other simulation

results of $E_b = 0.014$ eV and $d = 3.740$ Å (Leenaerts et al., 2008). However, in this particular adsorption configuration, the E_b value is still considered to be too small and d too large, even though they are the most favorable one for adsorption, reflecting that CO undergoes weak physisorption on the intrinsic graphene. This indicates that the intrinsic graphene is insensitive to CO molecules.

Initial binding configurations	Intrinsic graphene		Al doped graphene		
	E_b (eV)	d (Å)	E_b (eV)	l (Å)	
CO graphene	T-B-T	-0.011	3.839	-4.978	1.964
	T-H-T	-0.012	3.805	-4.973	1.968
	H-T-H	-0.014	3.826	-4.613	3.755
	H-B-H	-0.009	3.857	-4.599	3.814
	B(C atom)-T-H	-0.011	3.855	-4.609	3.800
	B(O atom)-T-H	-0.016	3.768	-4.616	3.821
CO⊥graphene	T(O upwards)	-0.007	3.938	-4.979	1.961
	B(O upwards)	-0.007	3.935	-4.978	1.964
	H(O upwards)	-0.003	3.982	-4.975	1.965
	T(C upwards)	-0.004	3.952	-4.629	3.781
	B(C upwards)	-0.003	3.981	-4.607	3.783
	H(C upwards)	-0.005	3.942	-4.609	3.457

Table 1. Summary of results for CO adsorption on intrinsic graphene and Al doped graphene on different adsorption sites. The meaning of T, B and H are given in the caption of Fig. 3. In the table headings, d represents the distance between CO gas molecule and graphene layer, l represents the bond length of Al and C atom in CO gas molecule.

Upon substituting one carbon atoms by Al, the geometric structure of the doped graphene changes dramatically, as shown in Fig. 4. Figs. 4(a) and 4(b) represent the geometries of intrinsic and Al doped graphene after relaxation. As shown in Table 2 and Fig. 4(b), the Al doping results in l elongation from $l_{C-C} = 1.420$ Å to $l_{Al-C} = 1.632$ Å. This is associated with the distortion of hexagonal structures adjacent to the larger Al atom, similar to the restructuring in Al doped SWCNTs (Wang et al., 2007).

When a CO molecule is adsorbed on the Al-substituted graphene, there also exists twelve possible adsorption sites similar to the CO adsorption on intrinsic graphene shown in Fig. 3. These are taken as initial configurations. After relaxation, the configuration in Fig. 3(d) has the most stable relaxed structure. The adsorption of CO causes a structure change in the Al doped graphene dramatically, resulting in an expansion of l_{Al1-C2} from 1.632 to 1.870 Å while l_{Al1-C4} elongates from 1.632 to 1.915 Å. The corresponding distance between the CO molecule and Al atom in the Al doped graphene is 1.964 Å, being much shorter than 3.767 Å in the intrinsic graphene system. Moreover, the E_b of CO in the Al doped graphene system is 4.979 eV, which is over 60 times larger than that of CO in the intrinsic graphene system. Comparing with the E_b in other systems, such as $E_b = 1.280$ eV for CO adsorbed in the Al doped SWCNT systems (Wang et al., 2007), $E_b = 0.986$ eV in the B doped SWCNT systems (Wang et al., 2007) and $E_b = 0.201$ eV for CO adsorbed in B doped graphene etc, the Al doped graphene is energetically more favorable for CO adsorption. In other words, the Al doped graphene is much more sensitive to the CO adsorption among the aforementioned systems.

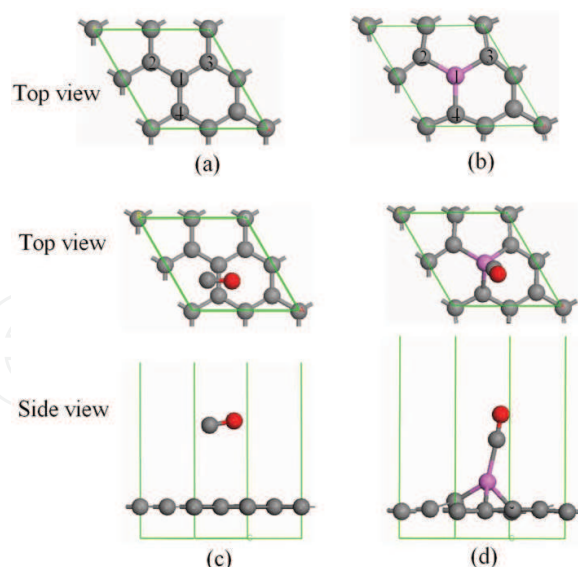


Fig. 4. Atomic configurations of intrinsic graphene and Al doped graphene before and after adsorption of CO gas molecule where one Al atom dopes in site 1, and sites 2, 3 and 4 are C atoms near the doped Al atom. (a) and (b) are the relaxed configurations of intrinsic graphene and Al doped graphene without adsorption. (c) and (d) are the preferred configurations after CO adsorption for intrinsic graphene and Al doped graphene, respectively. (Reproduced with permission from Ref. (Ao et al., 2008). Copyright 2008, Elsevier)

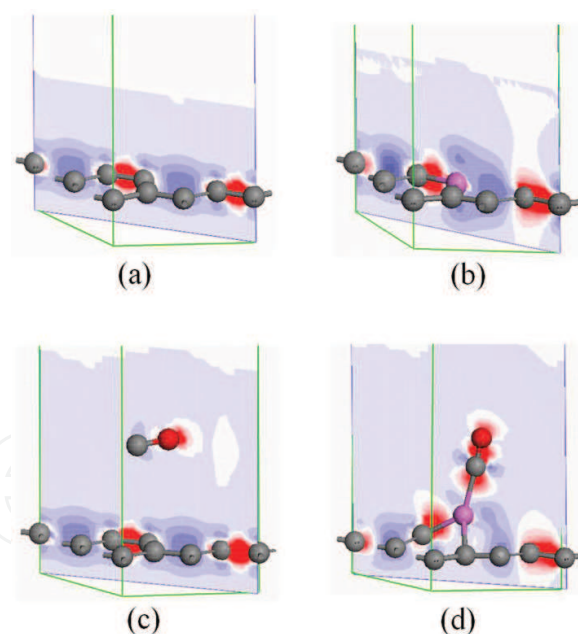


Fig. 5. Images of the electronic density difference for intrinsic graphene (a), Al doped graphene (b), CO-graphene system with preferred configuration (c) and CO-Al doped graphene system with preferred configuration (d). The red region shows the electron accumulation, while the blue region shows the electron loss. (Reproduced with permission from Ref. (Ao et al., 2008). Copyright 2008, Elsevier)

Furthermore, in order to investigate the changes of electronic structures in graphenes caused by the physi- or chemisorption of CO molecule, the net electron transfer (Q) from either the

System	Configuration	Bond	Bond length l (Å)	Q (e)
Intrinsic graphene	Fig. 4(a)	C1-C2	1.420	0.003
		C1-C3	1.420	
		C1-C4	1.420	
	Fig. 4(c)	C1-C2	1.420	
		C1-C3	1.421	
		C1-C4	1.421	
Al doped graphene	Fig. 4(b)	Al1-C2	1.632	0.027
		Al1-C3	1.632	
		Al1-C4	1.632	
	Fig. 4(d)	Al1-C2	1.870	
		Al1-C3	1.910	
		Al1-C4	1.915	

Table 2. Some structure parameters of intrinsic graphene and Al doped graphene before and after adsorption of CO molecule. Q denotes electrons transferred from the graphene layer to CO molecule, measured in the electronic charge e .

intrinsic or the Al doped graphene to the polar CO molecules had been calculated by Mulliken analysis, where Q is defined as the charge variation caused by the CO absorption. As listed in Table 2, $Q = 0.027 e$ in the Al doped graphene is almost an order of magnitude larger than $0.003 e$ in the intrinsic graphene. This supports the notion that the Al doping influences the electronic properties of graphene substantially. This can also be verified by the difference of electronic densities between the intrinsic and Al doped graphenes with and without the CO adsorption as shown in Fig. 5. In the figure, the red and blue regions represent the areas of electron accumulation and the electron loss, respectively. Fig. 5(a) indicates the bond in the intrinsic graphene is of covalent nature because the preferential electron accumulation sites are mainly located within the bond rather than heavily centered on a particular atom. However, the electron density distribution along the covalent Al-C bonds has been significantly altered due to the difference in electron affinity of Al and C atom [Fig. 5(b)]. Physisorption of CO on the intrinsic graphene does not alter the electron distribution for both CO molecule and graphene, implying the weak bonding characteristics. It is discernable that electronic polarization is induced by the preferential accumulation of electrons on O in CO molecules [Fig. 5(c)]. As distinct from the CO absorption on the intrinsic graphene, the chemisorption of CO on Al doped graphene leads to significant electron transfer from the graphene to CO molecule [Fig. 5(d)]. In this case, the electrons not only accumulate on the O atom but also on the C atom of the molecule bond with the doped Al atom. The final position of Al atom in the chemisorbed CO-Al-graphene complex is thus a direct consequence of the maximized degree of sp^3 orbital hybridization with neighboring C atoms from both the graphene layer and CO molecule. This is evidential because the red lobes around C atoms in Fig. 5(d) are both pointing towards Al atom.

To further determine the effects of CO absorption on electrical conductivity, DOS for the both systems with and without the absorption were calculated. As shown in Figs. 6(a) and (b), the Al doping in graphene enhances its electrical conductivity by shifting the highest DOS peak to just below the Fermi level E_f , which also leads to the reduction of band gap E_g . This indicates that the doped Al atom induces shallow acceptor states in graphene like B atom in SWCNs, thus enhancing its extrinsic conductivity (Peng & Cho, 2003). When the CO molecule adsorbed

on the intrinsic and doped graphene surfaces, the total DOSs are shown in Figs. 6(c) and 6(d). In the intrinsic graphene, the DOS of CO-graphene system near E_f have no distinct change, and the conductivity change is barely observable. It implies that the intrinsic graphene would not be an ideal CO gas sensor. However, for the Al doped graphene with the most stable chemisorbed CO configuration [Fig. 6(d)], not only the highest DOS peak shifts over the E_f , but also the DOS value increases dramatically. This results in an E_g closure [Fig. 6(d)] where E_g of the Al doped graphene is 0.18 eV without adsorption and the E_g becomes zero with adsorption. It suggests that extra number of shallow acceptor states have been introduced when the Al doped graphene interacts with the highly polar CO molecule. As a result, the chemisorbed CO on the Al doped graphene gives rise to a large increase in the electrical conductivity of the doped graphene layer. By detecting the conductivity change of the Al doped graphene systems before and after the adsorption of CO, the presence of this toxic molecule can be detected sensitively. Therefore, the Al doped graphene is a promising sensor material for detecting CO molecules. However, desorption of CO molecule from the Al doped graphene is difficult due to the strong bonding of Al-CO (Peng et al., 2004). This can be solved by applying an electric field F to reactivate the sensor materials (Hyman & Medlin, 2005).

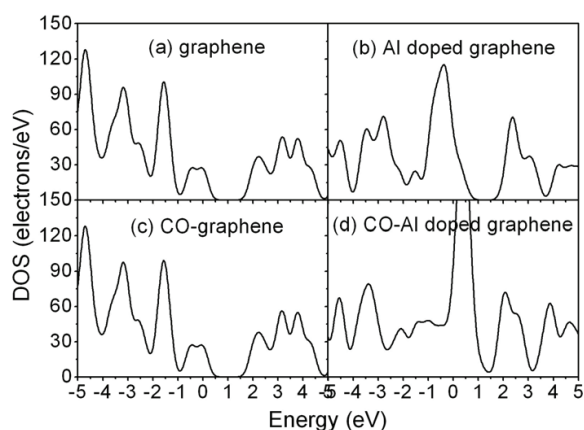


Fig. 6. Electronic density of state (DOS) of intrinsic graphene (a), Al doped graphene (b), CO-graphene system with preferred configuration (c) and CO-Al doped graphene system with preferred configuration (d). (Reproduced with permission from Ref. (Ao et al., 2008). Copyright 2008, Elsevier)

2.4 The effect of electric field on the adsorption/desorption behaviours of CO molecules

The first theoretical work with quantum mechanical calculations on electric field F inducing adsorption/desorption was studied for N_2 molecule on Fe(111) surface (Tomanek et al., 1985). Recent simulation works on the effects of F on: (1) the adsorption and dissociation of oxygen on Pt(111) (Hyman & Medlin, 2005), (2) electronic structure of Au-XO(0,-1,+1) ($X = C, N$ and O) (Tielens et al., 2007), and (3) vibrational frequencies of CO on Pt(111) (Lozovoi & Alavi, 2007) showed that F could induce some new physical phenomena by changing their electronic properties (McEwen et al., 2008).

Therefore, it is of interest to investigate how F influences the adsorption/desorption behaviours of CO on Al-doped graphene. Here, the favorable adsorption configurations of CO on Al-doped graphene under different F had been determined by DFT calculation, and the effects of F on the corresponding interaction between CO and Al-doped graphene will be further discussed. All DFT calculations were performed using Dmol³ code with the same settings as above in the section 2.3 (Delley, 1990; 2000).

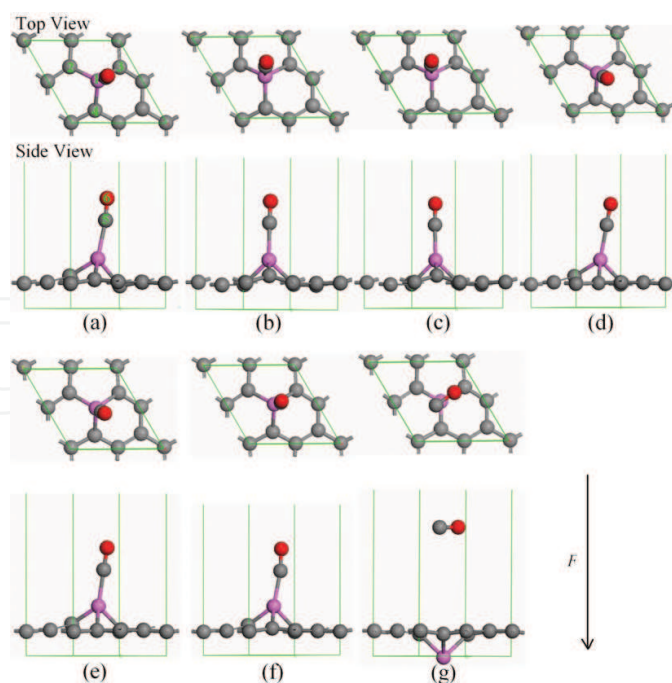


Fig. 7. The favorite adsorption configurations under different F . Atomic structures when $F = -0.03$ a.u. (a), $F = -0.02$ a.u. (b), $F = -0.01$ a.u. (c), $F = 0$ (d), $F = 0.01$ a.u. (e), $F = 0.02$ a.u. (f), (g) stable structure cannot be gotten when $F = 0.03$ a.u. and this structure is the configuration after 200 geometry optimization steps. The direction of the positive F is pointed out by the arrow. In the figure, gray, pink and red spheres are C, Al and O atoms, respectively. One Al atom dopes in site 1 and sites 2, 3 and 4 are C atoms near the doped Al atom, sites 5 and 6 are C and O atoms in the CO molecule. (Reproduced with permission from Ref. (Ao et al., 2010a). Copyright 2010, Elsevier)

In the calculations, all atoms were allowed to relax. Al-doped graphene structures were obtained through substituting one C atom in the graphene supercell by an Al atom as shown in Fig. 7. In this case, the concentration of the doped Al in graphene is 12.5% atomic ratio. For CO adsorption on Al-doped graphene, there are two highly symmetric adsorption configurations: (1) CO molecule resides parallel to the graphene surface, and (2) CO molecule resides perpendicular to the graphene surface. The detailed structures are similar as in the literature [Fig. 1 in Ref. (Ao et al., 2008)]. The $E_b(F)$ of CO molecule on Al-doped graphene under F can be determined by (Acharya & Turner, 2007),

$$E_b(F) = E_{CO+graphene}(F) - [E_{prot}(F) + E_{CO}(F)]. \quad (14)$$

where the subscripts CO+graphene, prot, and CO denote the adsorbed system, the initial isolated graphene with Al atom protruding from the graphene surface and the CO molecule, respectively. In the simulation, F had been chosen in the range of $-0.03 \sim 0.03$ a.u. (1 a.u. = 51 V/Å) and its positive direction is pointed out by the arrow in Fig. 7. Note that the length of the vacuum layer along the direction of normal to the graphene layer in the simulation system is about 15 Å. Thus, the maximum voltage required to induce the electric field with intensity of 0.03 a.u. is about 23 V, which can be easily realized in actual applications.

E_b of the CO/graphene systems with all possible adsorption configurations in the presence of F is listed in Table 3. Based on the calculated E_b values, the corresponding favourite adsorption configurations under different F are present in Fig. 7 where the CO molecule always takes

Initial configurations		F (a.u.)					
		-0.03	-0.02	-0.01	0	0.01	0.02
CO graphene	T-B-T	-0.966	-0.740	-0.631	-0.654		
	T-H-T	-0.906	-0.773	-0.664	-0.559	-0.370	
	H-T-H	-0.977	-0.746	-0.566	-0.199	-0.354	
	H-B-H	-0.952	-0.740	-0.618	-0.185	-0.356	
	B(C atom)-T-H	-0.865	-0.719	-0.650	-0.195		
	B(O atom)-T-H	-0.982	-0.692	-0.580	-0.202	-0.354	
CO⊥graphene	T(O upwards)	-0.895	-0.692	-0.593	-0.565	-0.379	-0.291
	B(O upwards)	-0.958	-0.776	-0.664	-0.564	-0.419	-0.280
	H(O upwards)	-0.968	-0.763	-0.648	-0.561	-0.372	
	T(C upwards)	-0.171	0.066	0.212	-0.215	-0.389	
	B(C upwards)	-0.242	0.068	0.253	-0.193		
	H(C upwards)	-0.245	0.111	-0.208	-0.195	-0.416	

Table 3. Summary of adsorption energy E_b of CO adsorption in eV on Al-doped graphene with different adsorption sites under different F where an Al atom replaces one C atom of the unit cell. There are twelve possible configurations for CO adsorption on Al-doped graphene, similar as in Ref. (Ao et al., 2008). T, B and H denote top site of C atoms, bridge site of C-C bond and hollow site of carbon hexagon, respectively. The blank space in the table denotes that there is no equilibrium structure in this situation.

the top site of the doped Al atom. From Table 3, the most stable structures were obtained from the initial arrangements of T-B-T, H-T-H, H-B-H, B(O atom)-T-H, B(O upwards) and H(O upwards) when $F = -0.03$ a.u., T-B-T, T-H-T, H-T-H, H-B-H, B(C atom)-T-H, B(O upwards) and H(O upwards) when $F = -0.02$ a.u., T-B-T, T-H-T, H-B-H, B(C atom)-T-H, B(O upwards) and H(O upwards) when $F = -0.01$ a.u., T-B-T, T-H-T, T(O upwards), B(O upwards) and H(O upwards) when $F = 0$, H-T-H, H-B-H, B(O atom)-T-H and B(O upwards) when $F = 0.01$ a.u., T(O upwards) and B(O upwards) when $F = 0.02$ a.u. where the letters T, B and H denote the sites of atom and CO molecule center on the graphene ring, respectively. Note that in Table 3, the error range of E_b for the favourite adsorption configurations from different initial arrangements above under a given F is within 5%.

	$F = -0.03$	$F = -0.02$	$F = -0.01$	$F = 0$	$F = 0.01$	$F = 0.02$
l_{Al1-C2}	1.863	1.911	1.913	1.872	1.883	1.898
l_{Al1-C3}	1.930	1.907	1.907	1.910	1.915	1.930
l_{Al1-C4}	1.883	1.861	1.865	1.916	1.922	1.921
l_{Al1-C5}	2.046	2.009	1.985	1.964	1.950	1.950
l_{O6-C5}	1.136	1.145	1.153	1.164	1.174	1.188

Table 4. Structure parameters of the favorite adsorption configuration under different F shown in Fig. 7. The unit of F and bond length l are respectively a.u. and Å, which is not shown in the table for clarity.

The corresponding parameters of the stable atomic structures after adsorption in Fig. 7 are listed in Table 4. The results show that the field induces slight atom structure deformation and the top site of the doped Al atom is always the favourable adsorption site. However, the

desorption of CO from the Al-doped graphene occurs when $F = 0.03$ a.u. due to the large upward force on CO molecule induced by electrical field as shown in Fig. 7(g), while the Al atom goes below the graphene layer due to the downward force on the positive charged Al atom. The configuration in Fig. 7(g) was obtained after 200 geometry optimization steps to demonstrate the desorption configuration.

Fig. 7 presents that the Al atom protrudes from the graphene surface after CO adsorption. However, the Al-doped graphene was found as a planer configuration before the adsorption. After the final adsorption configuration for CO on the Al-doped graphene was obtained, we removed the adsorbed CO and optimized the geometry of the Al-doped graphene. The result showed that the protruded Al-doped graphene layer could not return to the initial planer state and has a lower energy. This means that the planar Al-doped graphene is metastable, and there should be an energy barrier that prevents the Al-doped graphene transiting from the planer state to the protruding configuration. A force in the vertical direction would induce the transition. In this way, the adsorption energies of CO on Al-doped graphene layer in the presence of different electrical field intensities are defined as Eq. 14 and are given in Fig. 8.

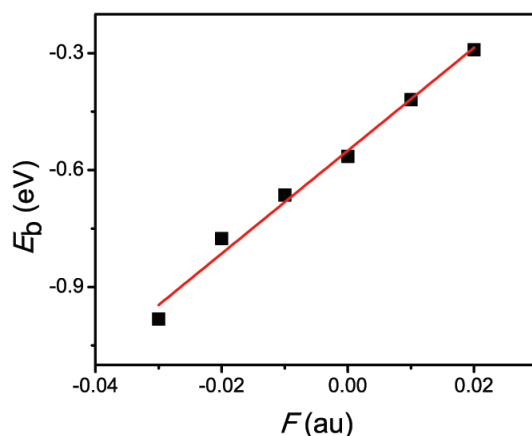


Fig. 8. $E_b(F)$ function of CO molecule adsorbed on Al-doped graphene. The squares are DFT results and the line is the fitted line to guide the eyes. (Reproduced with permission from Ref. (Ao et al., 2010a). Copyright 2010, Elsevier)

In Fig. 8, $E_b(F)$ increases nearly linearly as F increases. Therefore, the adsorption can be significantly strengthened by the negative F , while be weakened by the positive F . As F further increases, such as when $F \geq 0.03$ a.u., desorption occurs due to the electrostatic interaction as shown in Fig. 7(g). The approximate linear relationship between E_b and F can be explained by the first-order Stark effect (Hyman & Medlin, 2005). Thus, the highly positive F can be used to reactivate the sensor material for repetitious application.

On the other hand, in Table 4, as F increases, bond length l_{O6-C5} increases while l_{Al1-C5} reduces where the atom index is shown in Fig. 7. Such variations can be explained by Blyholder model (Koper & van Santen, 1999). The isolated CO molecule is bonded through sp_z hybrid orbital of a C atom and p_z orbital of an O atom. Therefore, a σ bond is formed while the interaction between p_x and p_y orbitals of the C and O atoms produces two π bonds (Blyholder, 1964). However, a lone pair of electrons on the O $2s$ orbital and a lone pair in the C sp_z hybrid orbital are left, forming a coordinate bond in a complex with a suitable acceptor orbital such as a p orbital on Al with a σ bond. It is believed that the back donation from a metal p orbital to the antibonding π^* molecular orbital of the CO ligand stabilizes the bond by removing the excess electrons. Such a σ orbital can be considered to be a bonding orbital for

C-O, but as an antibonding orbital for the Al-CO bond. Therefore, depopulating this orbital (donation) elongates l_{O6-C5} but shortens l_{Al1-C5} . In general, Fermi level E_f of a neutral Al lies between σ and π^* levels of CO (Wang et al., 2007). Applying a positive F lowers the energy levels of CO comparing to those of the Al-doped graphene (Lozovoi & Alavi, 2007), resulting in the π^* energy level moving towards E_f , whereas the σ level moves away. Thus, a positive F suppresses donation but enhances back donation, leading to a smaller l_{Al1-C5} and a larger l_{O6-C5} .

	$F = -0.03$	$F = -0.02$	$F = -0.01$	$F = 0$	$F = 0.01$	$F = 0.02$
Al1	0.968	0.957	0.927	0.896	0.866	0.829
C2	-0.341	-0.313	-0.286	-0.363	-0.358	-0.332
C3	-0.362	-0.317	-0.294	-0.275	-0.260	-0.229
C4	-0.323	-0.370	-0.370	-0.267	-0.249	-0.267
C5	-0.040	-0.056	-0.076	-0.101	-0.124	-0.147
O6	0.078	0.008	-0.058	-0.128	-0.197	-0.273
Q	0.038	-0.048	-0.144	-0.229	-0.312	-0.410

Table 5. Charges of atoms near the doped Al atom in CO/graphene system as well as charge transfer Q between the graphene and the CO molecules under different F , obtained by Mulliken analysis. The unit of the atom charge is one electron charge $|e|$ and that of F is a.u.

Table 5 lists: (1) the charges of C and Al atoms as well as the CO molecule, and (2) the charge transfer Q between the graphene and the CO molecule under different F obtained by Mulliken analysis. As F increases, the electron numbers of Al1, C5, and O6 increase while those of atoms C2, C3, and C4 decrease. This is because electrons flow from the C atoms in the graphene layer to atoms of Al1, C5 and O6 above the graphene layer with increasing F . This agrees with the reported phenomena where the negative F enhances adsorption while the positive F has a counter effect (Hyman & Medlin, 2005). As F increases, the effects result in a shorter l_{Al1-C5} , and a longer l_{O6-C5} due to the reduction of the attraction between C5 and O6. The trends of l_{Al1-C5} and l_{O6-C5} variations are consistent to the results shown in Table 4.

The electronic distribution under different F is displayed in Fig. 9. The bond between the CO and the graphene system in the figure is covalent because the preferential electron accumulation sites mainly localize in the bond rather than centralize on a particular atom. However, due to the different electronegativity of C, Al and O atoms, electrons lean to the C atom for Al1-C5 bond and O atom for C5-O6 bond. Furthermore, with increasing F , more electrons transfer from the doped graphene to the CO where the lost electrons are all from Al (Table 5). The images in Fig. 9, where the red regions around CO become larger and thicker, also confirm that Q increases with increasing F .

2.5 The effect of temperature on the adsorption/desorption behaviours of CO molecules

The favourable CO adsorption site on the Al doped graphene was identified through DFT calculations (Ao et al., 2008). But it was still far to be optimized for actual applications. In particular, the effect of temperature T on the adsorption/desorption behaviours on the CO/graphene system is still unclear. Based on the DFT results and thermodynamic analysis at 0 K, the adsorption phase diagrams can be established. The Gibbs free energy of adsorption, ΔG_{ads} can be expressed as:

$$\Delta G_{ads}(T) = G_{ads}(T) - G_g(T) - G_{CO}(T), \quad (15)$$

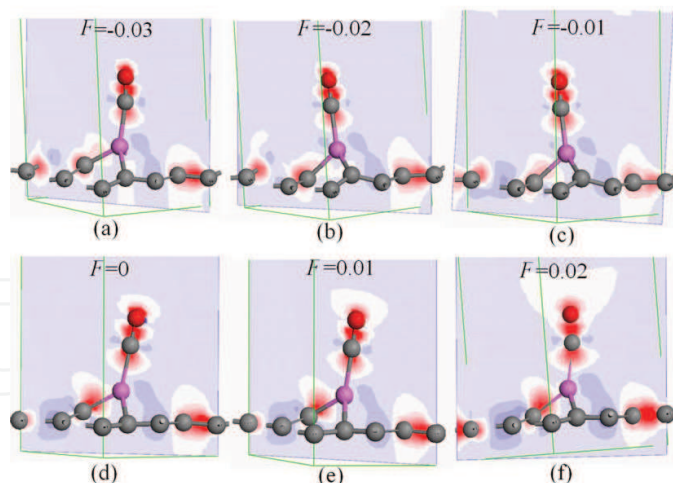


Fig. 9. Images of electron density difference of CO/graphene system under different F , the unit of F is a.u. The red region means electronic accumulation, while the blue region means electronic loss. (Reproduced with permission from Ref. (Ao et al., 2010a). Copyright 2010, Elsevier)

where $G_{ads}(T)$, $G_g(T)$ and $G_{CO}(T)$ are the corresponding Gibbs free energies of the adsorbed system, the Al doped graphene and the CO gas molecule at a particular T , respectively. Since the Gibbs free energy of the system before and after adsorption can be obtained with the DFT results, the adsorption-desorption transition could be determined with Eq. 15 theoretically.

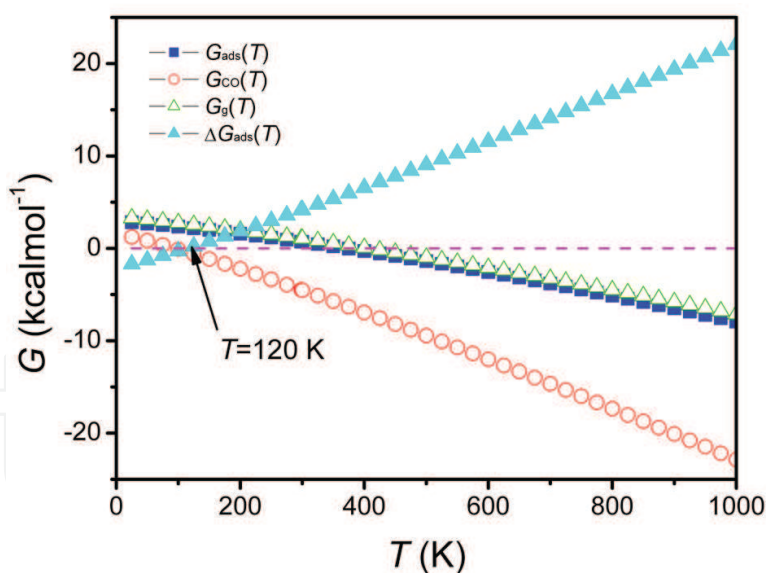


Fig. 10. The temperature dependent Gibbs free energy $G(T)$ functions where subscripts ads, g, and CO denote the adsorbed system, the isolated graphene and the CO molecules, respectively. And $G_{ads}(T)$ denotes Gibbs free adsorption energy, which is obtained in terms of Eq. 14. The symbols are all DFT results. (Reproduced with permission from Ref. (Ao et al., 2009b). Copyright 2009, RSC)

Subsequently, *ab initio* molecular dynamics (MD) calculations were performed under constant volume and constant temperature conditions (NVT) adopting GGA with the revised PBE method. The temperature effects on the atomic and electronic structures were calculated with

a time step of 1 fs at the temperatures from 300 to 450 K with an interval of 50 K. The simulation time t at the particular temperature was 2.5 ps where the total energy fluctuated in the range of 0.01%. MD calculation was based on the velocity Verlet algorithm (Verlet, 1967) for integration of the equation of motion. The implemented algorithm performs the Yoshida-Suzuki multiple-step numerical integration of varying quantity, depending on the choice of interpolation parameters (Suzuki, 1991; Yoshida, 1990). A key parameter in the integration algorithms is the integration time step. A common rule-of-thumb used to set the time step is that the highest frequency vibration should be sampled between 10 and 20 times in one cycle. In this system, the frequency is in the order of 10^{13} Hz, the time step was thus set as 1 fs within a reasonable range (Seitsonen et al., 2001). The temperature was controlled by algorithm of Nose (Nose, 1984). The thermostat employs a feedback loop between the instantaneous kinetic energy and the set temperatures. The rate of feedback is determined by the mass parameter, Q ($Q = 2$) (Loffreda, 2006; Spencer & Yarovsky, 2007; Todorova et al., 2007).

With the thermal desorption method, T dependent desorption time $\tau(T)$ function can be expressed as (Peng et al., 2004; Raaen & Ramstad, 2005)

$$\tau(T) = \nu_0^{-1} \exp[-E_b(T)/k_B T] \quad (16)$$

where k_B is the Boltzmann's constant (8.62×10^{-5} eV/K), and ν_0 is the attempt frequency of 10^{13} Hz for CO (Seitsonen et al., 2001). This thermal desorption method is close to the experimental conditions and it can be used to determine the thermodynamical properties of the adsorption systems (Raaen & Ramstad, 2005).

With the adsorption structures determined by the DFT calculations at an ideal condition, the phase diagram of adsorption/desorption for the CO adsorbed on the Al doped graphene as a function of temperature can be established with the atomistic thermodynamics described in Eq. 15. Such a simple approach allows the exploration of $\Delta G_{ads}(T)$ in an actual condition with respect to experiments. $\Delta G_{ads}(T)$, $G_{ads}(T)$, $G_g(T)$ and $G_{CO}(T)$ functions are plotted in Fig. 10. The results show that $\Delta G_{ads}(T)$ increases as T increases, and eventually becomes positive at $T_d = 120$ K where T_d is defined as the desorption temperature. In another word, the desorption of CO from the Al doped graphene occurs when $T_d > 120$ K at the ideal state with $\tau \rightarrow \infty$.

	$T = 0$	$T = 300$ K	$T = 400$ K	$T = 450$ K
l_{Al1-C2}	1.872	1.880	1.946	1.973
l_{Al1-C3}	1.910	1.961	1.972	1.993
l_{Al1-C4}	1.916	1.923	1.929	1.989
l_{Al1-C5}	1.964	1.982	2.097	4.590
l_{C5-O}	1.164	1.161	1.159	1.157

Table 6. Some structure parameters of CO molecule adsorbed on Al doped graphene at different temperature, where l is bond length in Å.

However, with *ab initio* MD calculation at $T = 300, 350, 400$ and 450 K for 2.5 ps to reach the equilibrium at each temperature, it was found that the desorption occurred at 450 K. The atomic configurations at the different temperatures are shown in Fig. 11 and their corresponding atomic structural parameters are listed in Table 6. The results show that T_d is between 400 and 450 K. Since both the data for MD simulation and atomistic thermodynamics come from the simulation, the difference of T_d caused by the simulation methodologies is

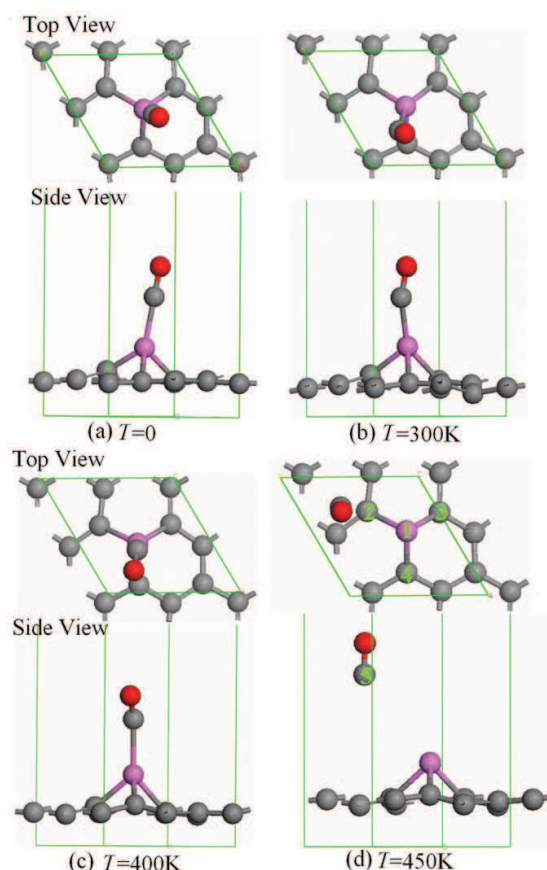


Fig. 11. Atomic structure of CO molecule adsorption in Al doped graphene at different temperature. For $T \neq 0$, the images are the configurations at simulation time $t = 2.5$ ps. In the figure, the uppermost atom is O atom, the third uppermost atom is Al atom, and the others are all C atoms. One Al atom dopes in site 1 and sites 2, 3 and 4 are C atoms near the doped Al atom, and site 5 is C atom in CO gas molecule. (Reproduced with permission from Ref. (Ao et al., 2009b). Copyright 2009, RSC)

limited and it could be ignored. It is believed that the difference is mainly induced by the short equilibrium time of $t = 2.5$ ps used in the MD simulation, which is much shorter than the actual situation.

$E_b(T)$ and $\tau(T)$ determined by Eqs. 13 and 16 are plotted in Figs. 12 and 13, respectively. Fig. 12 shows that $E_b(T)$ decreases linearly with T increasing. This is consistent with the classic Readhead formula (Readhead, 1962). In Fig. 13, $\tau(T)$ decreases exponentially with T increasing, showing $T_d \approx 420$ K at $\tau = 2.5$ ps. This is in agreement with the results obtained from MD simulation, in which the desorption occurs at $400 < T < 450$ K. In the experimental environment, the optimal τ is in an order of microsecond (μs) (Peng et al., 2004), and $\tau(400K) \approx 1 \mu s$ from Fig. 13, indicating that the gas sensor can be reactivated for repetitious applications by heating the materials up to 400 K. Note that the adsorption-desorption process is dynamic. Once the CO molecule is adsorbed, the adsorption state would be remained for a time of τ until the desorption occurs. During the adsorption period, electrical conductivity changes of the Al doped graphene can be detected.

Except for T_d , the temperature dependence of atomic structure and electrical properties are also critical information for gas detection. Table 6 lists the structural parameters calculated by *ab initio* MD at 300, 400 and 450 K, respectively. As T increases, Al-CO bond length l_{Al1-C5}

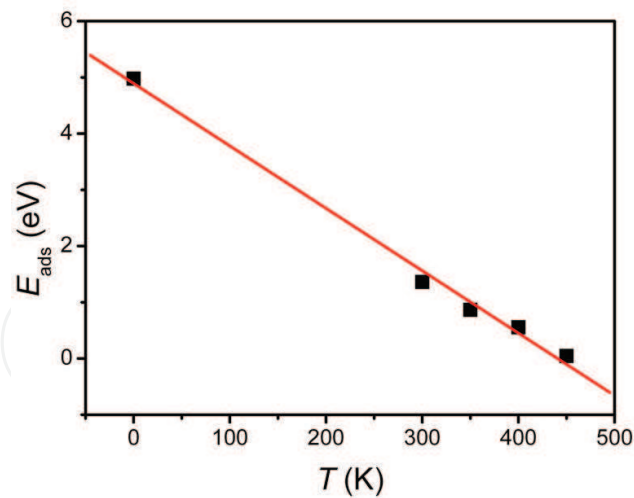


Fig. 12. Temperature dependent adsorption energy of CO molecule in Al doped graphene $E_b(T)$ function. The symbol ■ is the MD simulation result at $T = 0, 300, 350, 400, 450$ K. The solid line is the fitted linear function with the calculated data. (Reproduced with permission from Ref. (Ao et al., 2009b). Copyright 2009, RSC)

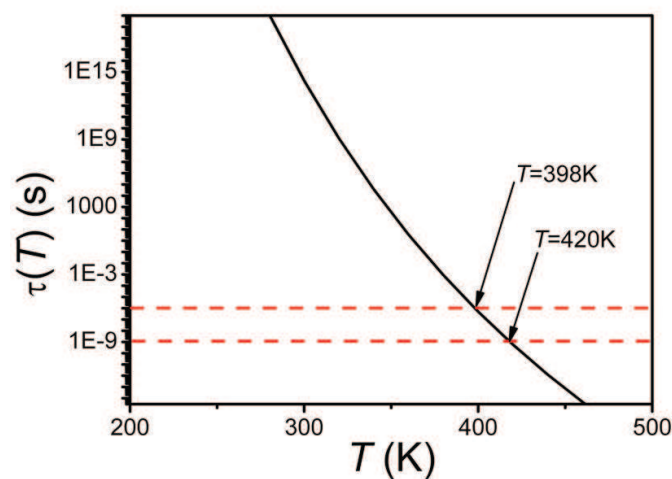


Fig. 13. Temperature dependent desorption time function $\tau(T)$ in terms of Eq. 16 where $E_b(T)$ function needed is from Fig. 12. The two temperatures 398 and 420 K are corresponding desorption temperature in MD simulation and actual situation. (Reproduced with permission from Ref. (Ao et al., 2009b). Copyright 2009, RSC)

increases, or the corresponding bond strength decreases. This is also evidenced by the $E_b(T)$ declination as shown in Fig. 12. When T further increases, the desorption of CO from the Al doped graphene occurs [Fig. 11(d)] where bond length of $l_{\text{Al1-C5}}$ changes sharply from 2.097 Å at 400 K to 4.590 Å at 450 K.

In order to better understand the results, Table 7 lists the charges of C atoms surrounding the doped Al atom, the doped Al atom and the CO molecule as well as charge transformation Q between the doped graphene and the CO molecule, which were obtained by Mulliken analysis. It exhibits that Q decreases as T increases and the Al atom loses electrons. The negative charges of the C atoms surrounding the doped Al also decrease. It results in the charge difference between the C and Al atoms decreases and the Al-C bond length in the

	$T = 0$	$T = 300$ K	$T = 400$ K	$T = 450$ K
Al1	0.896	0.833	0.765	0.613
C2	-0.363	-0.303	-0.324	-0.274
C3	-0.275	-0.287	-0.245	-0.276
C4	-0.267	-0.239	-0.255	-0.216
C5	-0.101	-0.089	-0.029	0.111
O	-0.128	-0.132	-0.127	-0.123
Q	0.229	0.221	0.156	0.012

Table 7. Charges of atoms surrounding doped Al atom and doped Al atom, and changes transferred Q form graphene to CO gas molecule at different temperature.

graphene layer elongates as T increases. This is consistent with the structure parameters change listed in Table 6. On the other hand, the electrons in C5 and O6 of the CO molecule also decrease with T increasing, and even C5 is positive at $T = 450$ K. Due to the static interaction, l_{C5-O6} decreases as T increases as shown in Table 6.

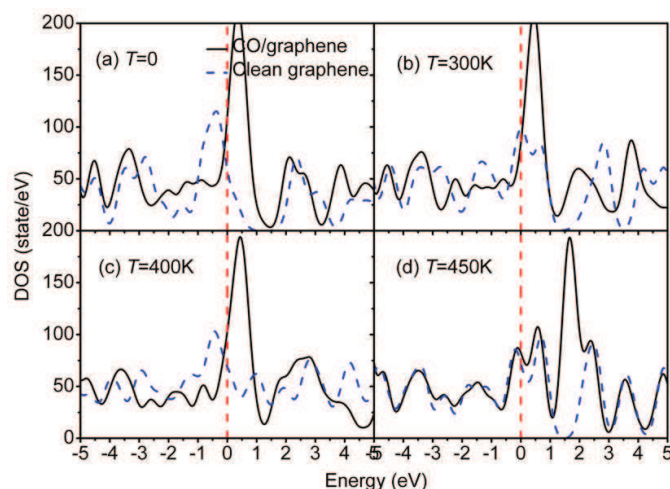


Fig. 14. Electronic density of state (DOS) of CO/graphene system at $T = 0$ (a), $T = 300$ K (b), $T = 400$ K (c) and $T = 450$ K (d). The dash lines denote the Fermi energy location and the dash curves are the DOS of the Al doped graphene. (Reproduced with permission from Ref. (Ao et al., 2009b). Copyright 2009, RSC)

To understand the effect of T on conductivity changes with and without the adsorption, the temperature dependence of DOS for the Al doped graphene and CO/graphene system are shown in Fig. 14. From Landauer formula (Tosatti et al., 2001), the number of bands crossing E_f determines the number of conduction channels or the conductivity of CO/graphene system (He et al., 2008; Mares & Van Ruitenbeek, 2005). Therefore, the largest conductivity change induced by the adsorption is found at $T = 400$ K. The performance of CO detection with this material is the best at $T = 400$ K based on the $\tau(T)$ function and conductivity change.

3. Application for efficient hydrogen storage

3.1 Hydrogen storage in Al substitutionally doped graphene

In recent years, hydrogen-based fuel systems have been considered to be a highly important topic of research for future energy schemes as hydrogen is a more efficient fuel in comparison

to the existing carbonaceous fossil fuels (Coontz & Hanson, 2004; Schlapbach & Züttel, 2001). Despite many recent technological developments in the hydrogen-based fuel systems, it is still an enormous challenge to have a safe and efficient reversible hydrogen storage system at ambient conditions (Schlapbach & Züttel, 2001). One possible way for hydrogen storage is an efficient and controllable adsorption/desorption system. Carbon based materials appear promising for such a purpose. Although several mechanisms of hydrogen storage through both physisorption and chemisorption have been proposed (Chandrakumar & Ghosh, 2008; Deng et al., 2004; Klontzas et al., 2008; Mpourmpakis et al., 2007; Nikitin et al., 2008), most of these efforts are far to reach the target of 6 wt% and binding strength of $-0.2 \sim -0.4$ eV/H₂ at ambient temperature and modest pressure for commercial applications specified by U.S. Department of Energy (DOE).

With DFT simulations, it was predicted that a single ethylene molecule can form a stable complex with two transition metals, thus adsorbing ten H₂ molecules and lead to a high storage capacity of ~ 14 wt% ((Durgun et al., 2006). In addition, the highest H₂ storage capacity of 13 wt% in a fullerene cage with twelve Li atoms capped onto the pentagonal faces was calculated (Sun et al., 2006). This system has average adsorption energy $E_b = -0.075$ eV/H₂. However, all the DFT results are in the ideal condition at the temperature of $T = 0$ K, their performances at the DOE specified operation conditions are unclear.

Since carbon nanostructures have high surface areas and thermal stability along with unique mechanical properties, improvement of their adsorption capacity by suitable modification would be of immense interest (Chandrakumar & Ghosh, 2008; Deng et al., 2004; Durgun et al., 2006; Klontzas et al., 2008; Mpourmpakis et al., 2007; Nikitin et al., 2008; Sun et al., 2006). Thus, hydrogen storage using carbon nanostructures is still an important research topic and deserves more attention. In this section, the potential of graphene as hydrogen storage materials through doping is investigated. The advantages of graphene are: (1) a large surface for hydrogen adsorption, (2) economical and scalable production (Li et al., 2008a), and (3) the strongest material ever measured (Lee et al., 2008).

AlH₃ and related aluminum hydrides as hydrogen storage materials have recently become the focus of renewed interest (Graetz et al., 2006; Li et al., 2007) due to their potentially large hydrogen capacity of ~ 10 wt%. These materials are thermodynamically unstable in ambient, but it is kinetically stable without much loss of hydrogen for years. Despite these excellent properties, extremely high pressure (exceeding 2.5 GPa) is required for hydrogen adsorption. While these hydrides possess a small negative enthalpy of formation (Graetz et al., 2006), for practical applications the large hydrogen desorption energy proves impractical. The origin of this energy barrier lies in the rather strong mixed ionic and covalent bonds (Graetz et al., 2006) formed between Al and H. Thus it is essential to significantly reduce the desorption energy.

There appears another way for Al atoms to store hydrogen i.e. to further decrease the interaction between Al and H. In this way, the weak chemisorption can be changed into strong physisorption. For hydrogen storage through physisorption, strong interaction between the H₂ molecule and the surfaces along with a large surface area for adsorption are required. The unique characteristics of graphene and Al for hydrogen storage lead to an investigation of the properties of Al doped graphene as a possible hydrogen storage candidate. It would be intriguing to understand the interaction between graphene, Al and H. In this work, the adsorption behaviour of H₂ in Al doped graphene was studied by DFT calculation. In addition, we processed the *ab initio* MD calculation to investigate the effects of temperature and pressure on the corresponding adsorption and desorption behaviours of this system.

All DFT calculations were performed with Dmol³ code (Delley, 1990). Previous studies (Cabria et al., 2008; Okamoto & Miyamoto, 2001) had shown that the LDA prediction of the physisorption energies of H₂ on the surface of graphite and carbon nanotubes were in good agreement with experiments. The reliability of LDA can be ascribed to the following facts (Cabria et al., 2008): (1) When the electron densities of H₂ and graphene overlap weakly, the nonlinearity of the exchange-correlation energy density functional produces an attractive interaction even in the absence of electron density redistribution; (2) The overestimated binding energy by LDA (Leenaerts et al., 2008; Lugo-Solis & Vasiliev, 2007) may compensate for the insufficient account of van der Waals interactions (Cabria et al., 2008). In contrast, DFT calculation using GGA produced a purely repulsive interaction. Using a GGA-PW91 functional, a repulsive interaction between H₂ and a graphene layer and also between H₂ and a (6,6) carbon nanotube was obtained (Tada et al., 2001). This contradicts the experimental findings (Sahaym & Norton, 2008). It was noted that LDA calculations well reproduce the empirical interaction potentials between graphitic layers and also in the other graphitic systems for distances near to the equilibrium separation although the LDA is not able to reproduce the long-range dispersion interaction (Girifacol & Hodak, 2002). Therefore, LDA had been selected in this work. To ensure that the calculated results were comparable, identical conditions were employed for the isolated H₂ molecules and the graphene, and also the adsorbed graphene system. The k-point was set to 6 × 6 × 2 for all slabs, which brought out the convergence tolerance of energy of 1.0 × 10⁻⁵ hartree (1 hartree = 27.21 eV), and that of maximum force is 0.002 hartree/Å.

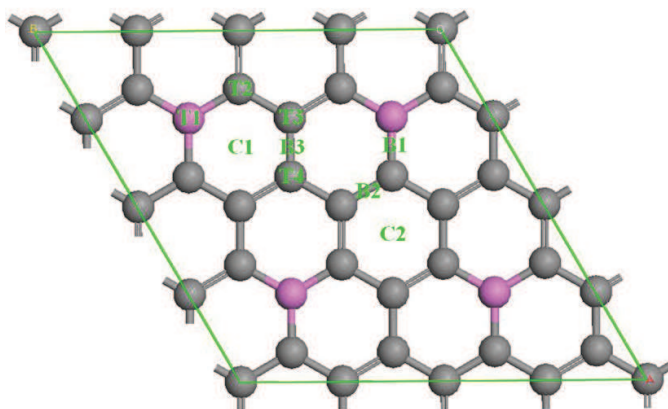


Fig. 15. Eight different adsorption sites on Al doped graphene. The gray and pink balls are respectively C and Al atoms. (Reproduced with permission from Ref. (Ao et al., 2009a). Copyright 2009, AIP)

In the simulation, three-dimensional periodic boundary condition was taken and H-H bond length was set to $l_{H-H} = 0.74$ Å, which is consistent with the experimental results (Lide, 2000). The graphene used in our simulation consist of a single layer of 2 × 2 supercell with a vacuum width of 12 Å to minimize the interlayer interaction. All atoms were allowed to relax in all energy calculations. The adsorption energy E_b between the H₂ gas molecule and graphene is defined as,

$$E_b = E_{H_2+graphene} - (E_{graphene} + E_{H_2}) \quad (17)$$

where the subscripts H₂+graphene, graphene, and H₂ denote the adsorbed system, isolated graphene and H₂ molecules, respectively.

For the Al doped graphene, the concentration of Al is 12.5 at% with the additional constrain that there is only one Al atom per graphene hexagonal ring (Fig. 15) to avoid Al atoms clustering on graphene (Krasnov et al., 2007). For H₂ adsorption on the Al doped graphene, there are 4 top sites of T1, T2, T3 and T4, and 3 bridge sites of B1, B2 and B3, and 2 center sites of C1 and C2, as shown in Fig. 15. (In this figure, a larger simulation cell is given in order to better display the different adsorption sites on the Al doped graphene. Fig. 16 reflects the actual simulation cell size.) At each adsorption site, there are two highly symmetrical adsorption configurations, namely H₂ molecule resides parallel or perpendicular to the graphene surface. Therefore, a total of 18 adsorption configurations for H₂ on the Al doped graphene are present.

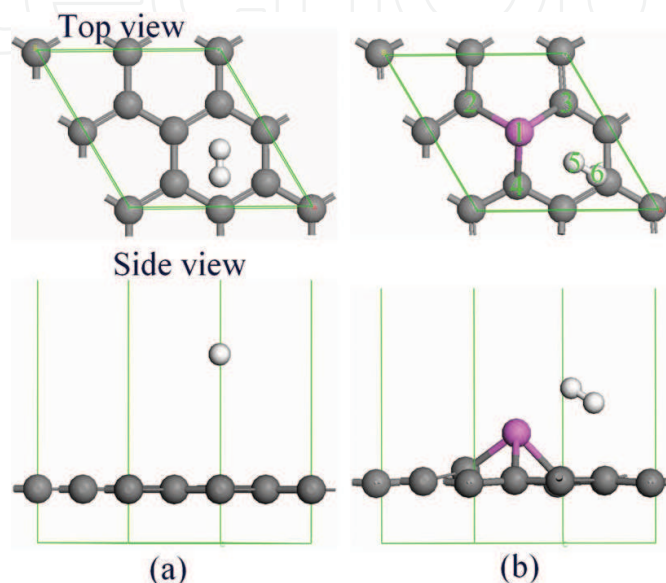


Fig. 16. The favorite adsorption configurations with 1 H₂ molecule adsorbed in intrinsic graphene (a), and in Al doped graphene (b). The white balls are H atoms. (Reproduced with permission from Ref. (Ao et al., 2009a). Copyright 2009, AIP)

Due to the periodicity of H₂ adsorbed in intrinsic graphene or Al doped graphene systems, we had selected the unit cell with the following conditions: eight C atoms and one H₂, or seven C atoms, one Al atom and one H₂ (see Fig. 16). If we placed a H₂ at any location of the cell, the distance from this H₂ to other H₂ molecules in the nearest cells is 4.920 Å. This large separation, compared to the bond length of H₂ (0.740 Å), would ensure that there is no interaction between H₂ molecules in the different cells (Arellano et al., 2000).

To calculate the H₂ adsorption capability of Al doped graphene at room temperature and modest pressure, we performed *ab initio* MD calculation with CASTEP (Cambridge Sequential Total Energy Package) code based on the structure obtained by DFT above, which utilizes plane-wave pseudopotential to perform the first principle quantum mechanics calculations (Degall et al., 2002). LDA with the Ceperley-Alder-Perdew-Zunger (CAPZ) function (Ceperley & Alder, 1980; Perdew & Zunger, 1981) was employed as exchange-correlation functions, cutoff energy $E_c = 280$ eV and k -points is $6 \times 6 \times 2$. In this work, the k -points of $6 \times 6 \times 2$ for all slabs have the energy convergence tolerance of 1.0×10^{-6} eV/atom. Such energy tolerance is small enough to ensure establishment of the actual equilibrium structure.

Each MD simulation was performed in NPT statistical ensemble, i.e. constant numbers of atoms N , pressure P and T , with $T = 300$ K and $P = 0.0001 \sim 1$ GPa. Time step of 1 fs was selected and simulation time t at a particular T was 2.5 ps where the total energy

fluctuation was in the range of 0.01%. The same t was selected for H₂S dissociation on the Fe(110) surface (Spencer & Yarovsky, 2007). A Verlet algorithm (Verlet, 1967) was used to integrate the equations of motion, with T controlled by algorithm of Nose (Nose, 1991), and P was controlled according to the Parrinello-Rahaman algorithm (Parrinello & Rahaman, 1981).

Initial configurations	Intrinsic graphene		Al doped graphene			
	E_b (eV)	d (Å)	E_b (eV)	l (Å)	d (Å)	
H ₂ graphene	T1	-0.136	2.845	-0.209	2.762	
	T2			-0.34	2.526	2.682
	T3			-0.407	2.588	2.486
	T4			-0.361	2.942	2.537
	B1	-0.139	2.817	-0.21	2.757	
	B2			-0.411	2.527	2.575
H ₂ ⊥ graphene	B3			-0.411	2.506	2.563
	C1	-0.159	2.635	-0.427	2.083	2.073
	C2			-0.188		2.657
	T1	-0.141	2.615	-0.153	2.622	
	T2			-0.284	2.427	2.749
	T3			-0.406	2.367	2.524
H ₂ ⊥ graphene	T4			-0.33	2.976	2.179
	B1	-0.142	2.620	-0.206	2.271	3.732
	B2			-0.412	2.468	2.595
	B3			-0.426	3.196	2.074
	C1	-0.148	2.425	-0.426	2.092	2.104
	C2			-0.24	3.117	2.468

Table 8. Summary of results for H₂ adsorption on intrinsic graphene and Al doped graphene on different adsorption sites. For H₂ adsorption on intrinsic graphene, there are 6 different adsorption sites as listed in the table. For H₂ adsorption on Al doped graphene, there are 18 different adsorption configurations as shown in Fig. 15. l represents the distance between Al and H₂. d represents the distance between H₂ molecule and graphene or Al-doped graphene.

After geometry relaxation, E_b values and the corresponding structural parameters of the 18 adsorption configurations for H₂ adsorbed in the intrinsic graphene are listed in Table 8. It was found that the most favorable configuration is H₂ adsorbed on the center site of the carbon ring with $E_b = -0.159$ eV as shown in Fig. 16(a) and the distance between H₂ and the graphene $d = 2.635$ Å. The results are consistent with other reported results of $E_b = -0.133$ eV and $d \approx 2.8$ Å (Okamoto & Miyamoto, 2001). The small magnitude of E_b (<0.1 eV) shows that the system is in the weak physisorption regime. It indicates that the intrinsic graphene is not suitable for hydrogen storage.

For the adsorption of H₂ on the Al doped graphene, the corresponding results are also listed in Table 8. In light of Table 8, the most favourable position with $E_b = -0.427$ eV for the H₂ molecule is shown in Fig. 16(b). The distance between H₂ and the doped Al, $l = 2.083$ Å while that between H₂ and carbon layer, $d = 2.073$ Å. As seen from Table 8, the interaction reaches the strongest when both l and d are minimized. The adsorption of H₂ in the Al doped graphene is much larger than that in other systems, such as $E_b = -0.41$ eV/H₂ in Ti-C₂H₄-graphene system (Durgun et al., 2006), and $E_b = -0.08$ eV/H₂ in

12-Li-doped fullerene (Sun et al., 2006). However, it still falls into the physisorption regime as the long distance between the doped graphene and the adsorbed H_2 . Therefore, this strong physisorption interaction would be ideal for hydrogen storage, which adsorbs more H_2 molecules.

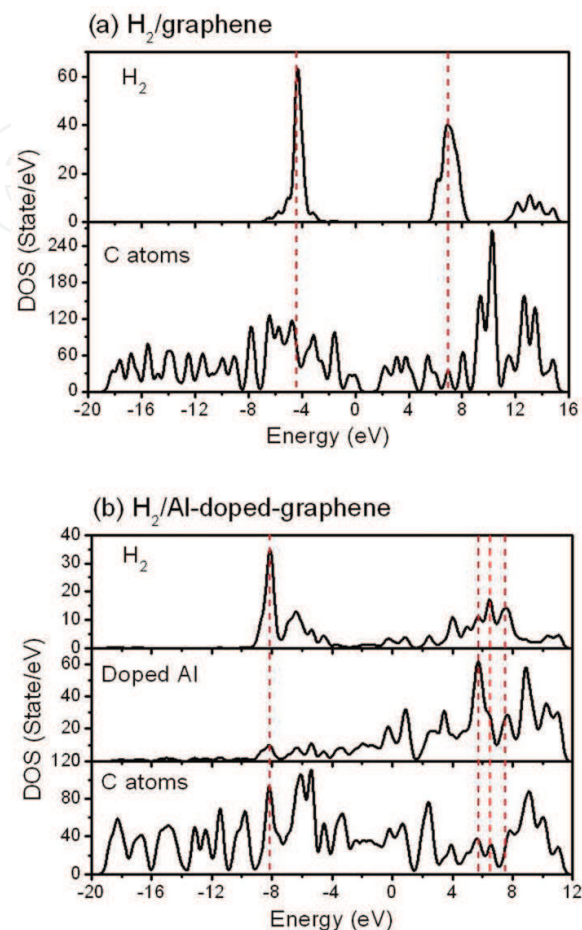


Fig. 17. Electronic density of states (DOSs) of adsorbed H_2 , doped Al and graphene for both the H_2 /graphene and H_2 /Al-doped-graphene systems as shown in panel (a) and panel (b), respectively. (Reproduced with permission from Ref. (Ao et al., 2009a). Copyright 2009, AIP)

To understand the enhancement effect of the doped Al on the H_2 adsorption, the DOSs of the adsorbed H_2 , the doped Al and the C atoms in both H_2 /graphene and H_2 /Al-doped-graphene systems were plotted and shown in Fig. 17. Fig. 17 (a) shows the DOSs of H_2 +graphene system. The main peaks of H_2 are located at -4.37 eV and 6.92 eV. However, the main peaks of intrinsic graphene are located between 9 and 13 eV. Therefore, the interaction between H_2 molecule and the intrinsic graphene is very weak because of non-overlapping of electrons in these substances, where E_b is small. On the other hand, for the H_2 /Al-doped-graphene system shown in Fig. 17(b), the main peaks of H_2 are located at -8.15 eV, 5.74 eV, 6.52 eV, and 7.51 eV, respectively. The bands of H_2 interact with both the doped Al and the C atoms synchronously at the positions indicated by the dash lines, showing a strong interaction between H_2 and the Al doped graphene where E_b is the largest. In addition, the doped Al changes the electronic structures of both H_2 and the graphene, and both their DOSs shift towards the lower energy. It exhibits that the H_2 /Al-doped-graphene configuration is a much more stable system.

Atom	Intrinsic graphene	Al doped graphene
Al1(C1)	0.001	0.292
C2	-0.002	-0.228
C3	0	-0.193
C4	0	-0.193
H5	-0.001	-0.001
H6	-0.001	0.021
Q	-0.002	0.019

Table 9. Charges of atoms in H_2 adsorbed in graphene system as well as charge transfer Q between graphene and H_2 molecule, obtained by Mulliken analyse. The unit of the atom charge is one electron charge e , which is elided here for clarity.

Table 9 shows the charge distribution in both the H_2 /graphene and H_2 /Al-doped-graphene systems using Mulliken analysis. Before and after H_2 adsorption, the charge variation for the former is little while it is significant for the latter. In addition, H6 has much more positive charge than H5. Thus, the interaction between H_2 and the Al doped graphene is mainly achieved through H6. The interaction between the band at the location of the highest peak of DOS plot of H_2 and that of C atoms implies a strong interaction between the H_2 and C atoms, as shown in Fig. 17(b).

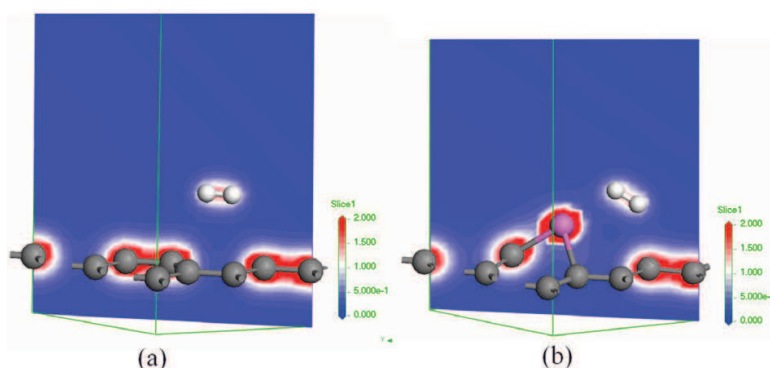


Fig. 18. Electron density distributions in the H_2 /graphene [panel (a)] and H_2 /Al-doped-graphene [panel (b)] systems. (Reproduced with permission from Ref. (Ao et al., 2009a). Copyright 2009, AIP)

The illustrations of electron density distribution for the H_2 /graphene and H_2 /Al-doped-graphene systems are shown in Fig. 18. In the system of H_2 /graphene [Fig. 18(a)], no electron exists in the region between H_2 and C layer while some electrons appear in the region among H_2 , Al atom and C layer in the system of H_2 /Al-doped-graphene [Fig. 18(b)]. This supports the notion that the H_2 /Al-doped-graphene possesses a much stronger H_2 adsorption ability.

After understanding the mechanism of the enhancement for H_2 adsorption in the Al doped graphene, it is important to determine how much H_2 molecules can be adsorbed on the 2×2 layer surface. We constructed an adsorption configuration with 3 H_2 molecules adsorbed in the three favourable C1 adsorption positions on the topside of the doped system. After geometry relaxation, the atomic structure is shown in Fig. 19(a). It has $E_b = -0.303$ eV/ H_2 , which satisfies the requirement of $E_b = -0.20 \sim -0.40$ eV/ H_2 at room temperature (Chandrakumar & Ghosh, 2008; Deng et al., 2004; Klontzas et al., 2008; Mpourmpakis et al.,

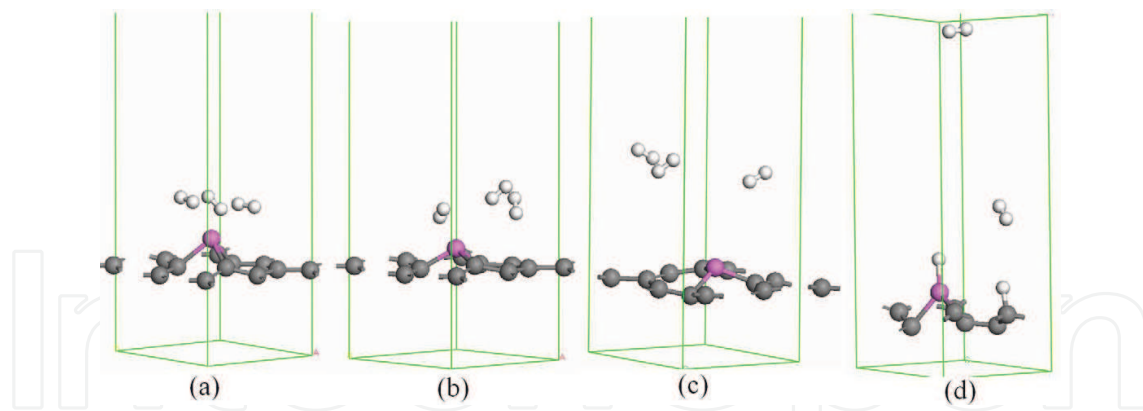


Fig. 19. Atomic configurations H_2 /Al-doped-graphene system at different temperature and pressure. (a) In the ideal condition with $T = 0$ K, (b) in the condition with $T = 300$ K and $P = 0.1$ GPa, (c) in the condition with $T = 300$ K and $P = 0.0001$ GPa, and (d) in the condition with $T = 300$ K and $P = 1$ GPa. (Reproduced with permission from Ref. (Ao et al., 2009a). Copyright 2009, AIP)

2007) set by DOE although the value of 5.1 wt% of H_2 adsorbed is slightly below the DOE's 6 wt% target.

In order to understand the effect of the adsorbed H_2 molecule number on the E_b , the configuration with 6 H_2 molecules adsorbed in the Al doped graphene in the favorable C1 adsorption positions on both sides was calculated. It is found that $E_b = -0.164$ eV/ H_2 , which is almost half of the E_b for above the case where the Al doped graphene adsorbed 3 H_2 on one side of graphene. In addition, the adsorption with 8 H_2 molecules in the Al doped graphene was also calculated, and it is found 2 H_2 molecules were released. In the other words, the interaction between H_2 molecules would weaken the adsorption on the doped graphene and the saturated number of H_2 molecules adsorption is 6. Note that E_b for the cases of 3 H_2 and 6 H_2 are respectively -0.303 eV/ H_2 and -0.164 eV/ H_2 , which is about twice for the case of 3 H_2 comparing with the case of 6 H_2 . This is because H_2 molecules were very weakly adsorbed below the graphene layer where the doped Al atom locates above the graphene layer.

It is well known that T and P have essential effects on hydrogen storage, where increasing P and decreasing T enhance the capacity of hydrogen storage. Thus, most studied systems are either under high P or at very low T (Sahaym & Norton, 2008), which may not be viable for mobile applications. For example, a storage capacity of 8 wt% for purified single wall carbon nanotubes (SWNTs) at 80 K with a hydrogen pressure of 13 Mpa (Ye et al., 1999) and a lower hydrogen storage capacity of 2.3 wt% at 77 K were reported (Panella et al., 2005). The hydrogen storage capacities in other carbon related materials, such as activated carbon (AC), single walled carbon nanohorn, SWNTs, and graphite nanofibers (GNFs) were also investigated (Xu et al., 2007). Although the AC had a capacity of 5.7 wt% at 77 K with $P = 3$ MPa, its capacity is $< 1\%$ at 300 K (Xu et al., 2007). Recent experimental results demonstrated that the intrinsic graphene has hydrogen storage capacity of 1.7 wt% under 1 atm at 77 K, and 3 wt% under 100 atm at 298 K (Ghosh et al., 2008). Thus, to meet the DOE target, it is necessary to study the adsorption and desorption behaviours of H_2 in the Al doped graphene at $T = 300$ K with different P . Therefore, the adsorption behaviours of $3H_2$ /Al-doped-graphene and $6H_2$ /Al-doped-graphene systems were calculated under 0.0001, 0.01, 0.1 and 1 GPa using *ab initio* MD simulation. For both the $3H_2$ /Al-doped-graphene and $6H_2$ /Al-doped-graphene systems, we found that all H_2 molecules were released at 0.0001 GPa [Fig. 19(c)]. However, there was only one H_2 molecule adsorbed in both the systems at 0.01 GPa, while the structure

of the doped graphene was completely destroyed with H and Al forming covalent bond at 1 GPa [Fig. 19(d)]. When $P = 0.1$ GPa, there are three H_2 left on the top side of the two Al doped systems [Fig. 19(b)]. Therefore, the Al doped graphene for hydrogen storage capacity at room temperature and 0.1 GPa is 5.13 wt% with $E_b = -0.260$ eV/ H_2 , satisfying the requirements of actual application. In addition, all the adsorbed H_2 molecules can be released when $P = 0.0001$ GPa.

3.2 Hydrogen storage in graphene with Al atom adsorption

Very recently, based on DFT calculations, Ca atoms adsorbed on graphene layers and fullerenes were found to result in high-capacity hydrogen storage mediums, which could be recycled at room temperature (Ataca et al., 2009; Yoon et al., 2008). In these systems, the adsorbed Ca atoms become positively charged and the semimetallic graphene changes into a metallic state, while the hydrogen storage capacity (HSC) can be up to 8.4 wt %. However, a recent report claimed that DFT calculations overestimated significantly the binding energy between the H_2 molecules and the Ca^{+1} cation centers (Cha et al., 2009). On the other hand, Al-doped graphene where one Al atom replaces one C atom of a graphene layer was reported as a promising hydrogen storage material at room temperature with HSC of 5.13 wt % (Ao et al., 2009a).

In this work, DFT was applied for studying the hydrogen adsorption on graphene with Al atom adsorption. The favourite adsorption configuration of Al atoms on single side and on both sides of a graphene layer have been determined. The obtained materials were studied for adsorption of H_2 molecules and we discuss its hydrogen storage properties.

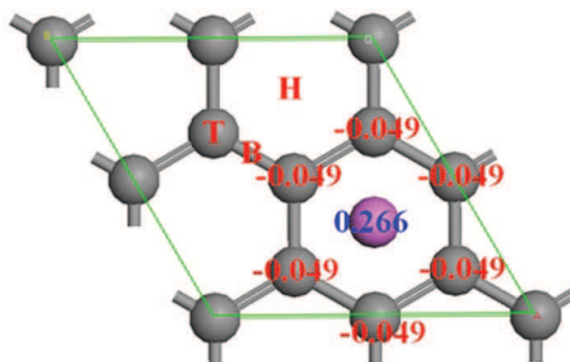


Fig. 20. Three different sites for an Al atom adsorbed on graphene. H, B and T denote the hollow of hexagon, bridge of C-C bond and top site of C atom, respectively. In addition, the charges of atoms near the adsorbed Al atom are also given, where the unit of charge is one electron charge e which is not given in the figure for clarity. The gray and pink balls in this figure and figures below are C and Al atoms, respectively. (Reproduced with permission from Ref. (Ao & Peeters, 2010b). Copyright 2010, APS)

LDA was used for all the calculations in this section. All DFT calculations were performed using the Dmol³ code (Delley, 1990). Double Numerical Plus polarization (DNP) was taken as the basis set. In this case, three-dimensional periodic boundary conditions were applied and the H-H bond length was set to $l_{H-H} = 0.74$ Å identical to the experimental value (Lide, 2000). The computational unit cell consists of a 2×2 graphene supercell with a vacuum width of 18 Å to minimize the interlayer interaction. As shown in Fig. 20, the supercell contains 8 C atoms. All atoms were allowed to relax in all calculations.

The binding energy of Al atoms onto graphene E_{b-Al} is defined as,

$$E_{b-Al} = [E_{nAl-graphene} - (E_{graphene} + nE_{Al})]/n \quad (18)$$

where $E_{nAl-graphene}$, $E_{graphene}$ and E_{Al} are the energy of the system with n Al atoms adsorbed on the graphene layer, the energy of the pristine graphene layer and the energy of one Al atom in the same slab, respectively. The binding energy of H_2 molecules onto Al-adsorbed graphene layer E_{b-H_2} is defined as,

$$E_{b-H_2} = [E_{iH_2+Al-graphene} - (E_{Al-graphene} + iE_{H_2})]/i \quad (19)$$

where the subscripts $iH_2+Al-graphene$, $Al-graphene$, and H_2 denote the system with i H_2 molecules adsorbed, isolated Al-adsorbed graphene and a H_2 molecule, respectively.

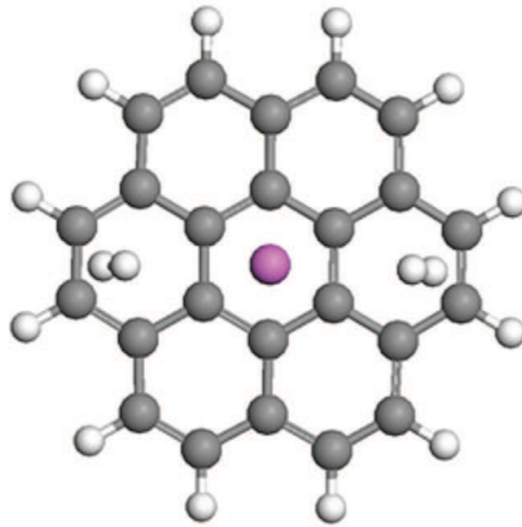


Fig. 21. A cluster model for 2 H_2 molecules adsorbed on graphene with an Al atom adsorbed on its one side. The white balls are hydrogen atoms in this figure and figures below. (Reproduced with permission from Ref. (Ao & Peeters, 2010b). Copyright 2010, APS)

To investigate the potential effects of different methodologies on our results, a calculation using the cluster model was carried out with both LDA and wave function approaches with the Møller-Plesset second order perturbation (MP2) within the Gaussian modules where the $6-331++G^*$ basis set was taken and maximum step size was set to 0.15 Å. Note that the cluster configuration shown in Fig. 21 was used because of the requirement of Gaussian modules, and the system was recalculated by LDA for purposes of comparison. In this calculation, a cluster with 24 carbon atoms and with 1 Al atom and 2 H_2 molecules adsorbed over the carbon surface was simulated where the dangling bonds of the C atoms at the boundary are terminated with H atoms.

On the basis of the published results, one may assume that the uptake capacity of hydrogen would increase if more metal atoms were adsorbed on the surface of a graphene nanostructure (Ataca et al., 2009; Liu et al., 2009). Furthermore, the binding between metal atoms and a surface would be strengthened if more charge is transferred between the metal atoms and the graphene nanostructure. Obviously, the binding can also be enhanced by adding more metal atoms with concomitant additional charges available for electronic transfer. However, metal atoms intend to aggregate into clusters when their concentration is large due to their high cohesive energies compared with those of metal atoms adsorbed on graphene, which

may significantly reduce the hydrogen uptake (Krasnov et al., 2007). For the Al, the cohesive energy is -3.39 eV (Gaudoin et al., 2002). To examine the validity of this assumption, a unit cell with eight C atoms and one Al atom was used in the present study, which is shown in Fig. 20. The ratio Al:C = 1:8 is quite moderate and moreover strictly obeys the doping rules for high coverage metals (Froudakis, 2001; Gao et al., 1998), which makes it possible for us to achieve a relatively high storage capacity. This rule ensures that the Al-Al distance is sufficiently large avoiding clustering of Al on graphene.

The favourite adsorption position of this Al atom on graphene is then determined. There are three different adsorption sites as shown in Fig. 20, which are the hollow of the carbon hexagon (H), the bridge of C-C bond (B), and the top site of the C atom (T), respectively. The Al-Al interaction is indeed negligible owing to the large distance of about 4.92 Å. It is found that the Al adsorbed at the H site has the lowest energy and is therefore the favourite adsorption configuration with a binding energy of -0.824 eV and the distance between Al and the graphene layer d_1 is about 2.079 Å. In Fig. 20, the charges of atoms near the adsorbed Al atom are given, which were obtained by Mulliken analysis. The adsorbed Al atom has a positive 0.266 e charge, while each C atom nearby has a negative charge -0.049 e . Note that the other two C atoms in the simulation cell contribute the rest of the electron charge to the negative C atoms. Therefore, the long distance of Al-Al, the relative strong bonding between the Al atom and the graphene layer, and the Coulomb repulsion between the Al atoms prevent metal aggregation on graphene.

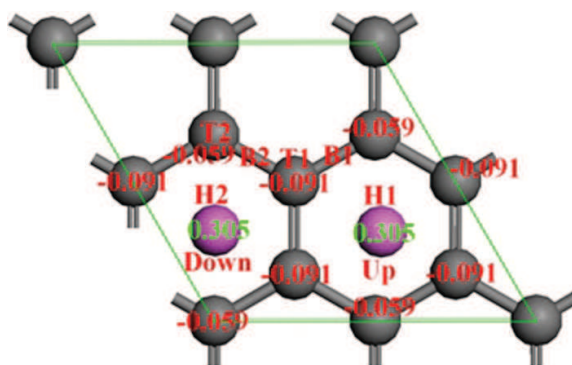


Fig. 22. Six different adsorption sites for the second Al atom on the other side of the graphene layer. The charges of atoms near the adsorbed Al atoms are also given, where the unit of charge is one electron charge e . (Reproduced with permission from Ref. (Ao & Peeters, 2010b). Copyright 2010, APS)

Due to the positive charge on the Al atoms and the negative charge on the carbon atoms, an electric field is induced between the Al atoms and the graphene layer, which in turn leads to a back transfer of charge from the graphene layer to the Al atom. Hence, by increasing Al coverage, adsorbed Al atoms would become less positively charged, which would decrease the Coulomb repulsion between the Al atoms, and eventually this may lead to metal aggregation. This also agrees with the doping rules (Froudakis, 2001; Gao et al., 1998). To further confirm the stability of Al atoms on graphene, the diffusion behavior of an Al atom on graphene was studied by the transition search (TS) method in order to obtain the diffusion barrier. It has been shown above that the most stable configuration of an Al atom on graphene corresponds to adsorption on the H site of graphene. Consequently, the diffusion scenario of an Al atom on graphene between two H sites is considered in order to study surface diffusion. Based on the TS calculation, it is found that the classical barrier for surface

diffusion is 0.104 eV. Notice that the calculated diffusion barrier corresponds only to a classical hopping model of diffusion. In practical cases, quantum tunneling effects should also be considered (Wu et al., 2009). In addition, because only a single Al atom is involved in the simulation cell, the Al-Al distance is kept unchanged. While in actual diffusion, the Al-Al distance would be shortened and repulsive Coulomb interaction among positively charged Al atoms would increase, leading to a significant increase of the diffusion barrier, which will prevent aggregation of adsorbed Al atoms on graphene.

Next the adsorption of Al atoms on both sides of the graphene layer is considered in order to increase the available surface area for hydrogen storage, since the charged metal atoms are the nucleation centres for hydrogen adsorption (Ataca et al., 2009; Liu et al., 2009; Yoon et al., 2008). As shown in Fig. 22, there are six different sites for the second Al atom to be positioned on the other side of the graphene layer. After geometry optimization of the six configurations, we found that the lowest energy configuration is realized for the second Al atom adsorbed on the H2 site with energy $E_{b-Al} = -1.096$ eV and the average E_{b-Al} for the two Al atoms is -0.960 eV. As shown in Fig. 22, the two Al atoms are positioned on two shoulder-by-shoulder carbon hexagons but on opposite sides of the graphene layer. The repulsive Coulomb interaction between the positively charged Al atoms on the upper and lower parts of the graphene plane is screened by the negative charge on the C-atoms. The graphene layer is now more negatively charged as compared to the previous single Al atom case, while the adsorbed Al atoms are more positively charged (the charges of the atoms on the Al and C atoms are given in Fig. 22). It leads to a stronger binding energy for the Al atoms on the graphene. In addition, $d_1 \approx 2.138$ Å which is slightly larger as compared to the case of single side adsorption which is counter intuitive. The reason is that the small increase of d_1 is a result of the Coulomb repulsion between the two positively charged Al atoms located above and below the graphene layer, which is screened by the charged graphene layer.

For the case of one H₂ molecule adsorbed on graphene with Al atoms adsorbed on a single side of graphene, the configuration after relaxation is shown in Fig. 23(a) where a 4×4 supercell is taken in order to better display the atomic structure, especially the adsorption site of the H₂ molecule. It indicates that the H₂ molecule would take the center site of equilateral triangles formed by adsorbed Al atoms. The vertical distance between the H₂ molecules and the graphene layer is $d_2 = 2.830$ Å, while d_1 decreases slightly to 2.060 Å, and the adsorption energy for the first H₂ molecule is $E_{b-H_2} = -0.182$ eV/H₂. In the figure, it shows that a parallelogram formed by the adsorbed Al atoms has two centre sites of equilateral triangles. However, due to the limitation of interaction among adsorbed H₂ molecules, H₂ would take just one of the two centre sites. When more H₂ molecules are adsorbed, the two centre sites would be both occupied as shown in Fig. 23(b) where two H₂ molecules are adsorbed. The adsorption energy for the second H₂ molecule is $E_{b-H_2} = -0.273$ eV/H₂, which gives an average adsorption energy for the two H₂ molecules of -0.227 eV/H₂. Fig. 23(c) gives the atomic structure of three adsorbed H₂ molecules. Two H₂ molecules take the two centre sites as in Fig. 23(b), the other H₂ molecule would take the top site of the Al atom. The distance of the three H₂ to the Al atom are respectively 2.786, 2.879 and 2.903 Å with average binding energy of -0.176 eV/H₂. If we further increase the number of H₂ molecules, after relaxation, the result shows that the fourth H₂ molecule cannot be adsorbed. Therefore, it is concluded that the maximum number of H₂ molecules adsorbed on a single side of a 2×2 graphene unit cell is three.

For the cases of one and two adsorbed H₂ molecules, it was found that the H₂ molecules are parallel to the graphene layer and all H₂ molecules are equidistant from the Al atoms. Once

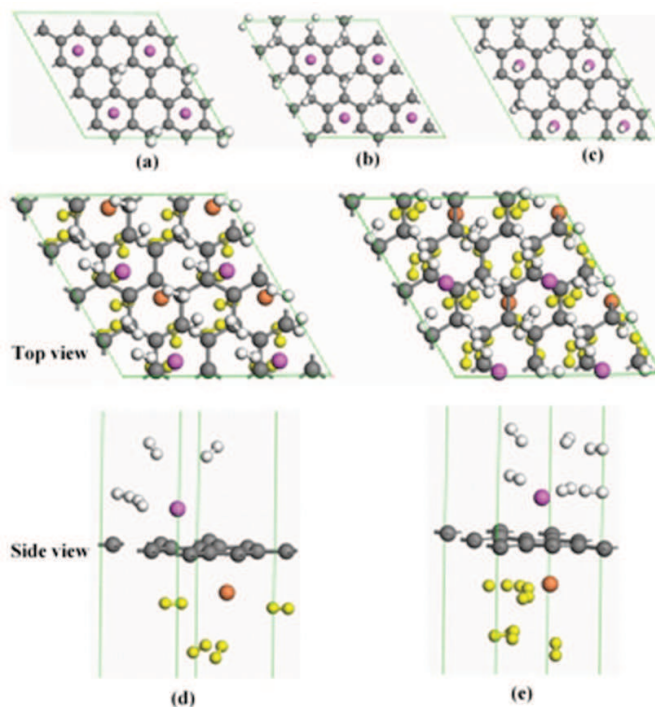


Fig. 23. Atomic structures of H₂ molecules adsorbed on Al-adsorbed graphene. (a) One H₂ molecule adsorbed on graphene with Al adsorbed on the single side, (b) two H₂ molecules adsorbed on graphene with Al adsorbed on a single side of graphene, (c) three H₂ molecules adsorbed on graphene with Al adsorbed on one side of graphene, (d) four H₂ molecules adsorbed on each side of graphene with Al adsorbed on its both sides, (e) six H₂ molecules adsorbed on each side of graphene with Al adsorbed on its both sides. In this figure, 4×4 supercells are plotted to better display the adsorption sites of the H₂ molecules. In (d) and (e), due to the Al atoms and H₂ molecules adsorbed on both sides of graphene, Al atoms and H₂ molecules below the graphene layer are shown as orange and yellow, respectively. Meanwhile, in order to show the two-layer adsorption arrangement of H₂ molecules, initial simulation cells of side view are also given in the nether part of (d) and (e). (Reproduced with permission from Ref. (Ao & Peeters, 2010b). Copyright 2010, APS)

the number of H₂ absorbed on each Al atom exceeded two, the absorbed H₂ molecules tend to tilt towards the Al atoms because of the increased positive charge of the Al atoms and the symmetry of the bonding configuration of the H₂ molecules. This phenomenon is similar to the case of adsorption of H₂ molecules on Ca-adsorbed graphene (Ataca et al., 2009).

In addition, it was noted that the E_{b-H_2} of the second H₂ molecule is much larger than that of the first one, i.e. it is about 50% larger. In order to understand this enhancement, PDOS of Al, C atoms and H₂ molecules are plotted and shown in Fig. 24. It was reported that the band broadening of the molecular level of H₂ below the Fermi energy indicates a significant H₂-H₂ interaction that in turn increases its binding energy to the substrate (Ataca et al., 2009). In this work, the same mechanism is found where the band broadening of about -6 eV appears in Fig. 24. In fact, the binding energy of the first H₂ molecule to the Al atom which prefers to be parallel to the graphene layer is generally small (Ataca et al., 2009).

Figure 25 displays the electron density of the system with one and two adsorbed H₂ molecules. Notice that there is non-zero electron density in the region between the graphene layer and the adsorbed Al atom. This is the reason why Al atoms are strongly adsorbed on the graphene

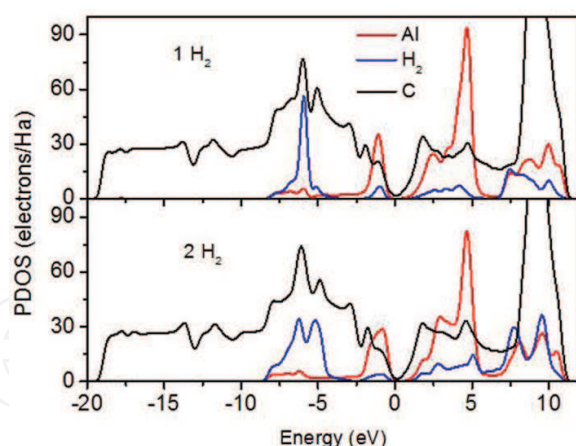


Fig. 24. PDOS of Al, H₂ and C in the systems of one and two H₂ molecules adsorbed on graphene with Al adsorbed on the single side. The Fermi level is at 0. (Reproduced with permission from Ref. (Ao & Peeters, 2010b). Copyright 2010, APS)

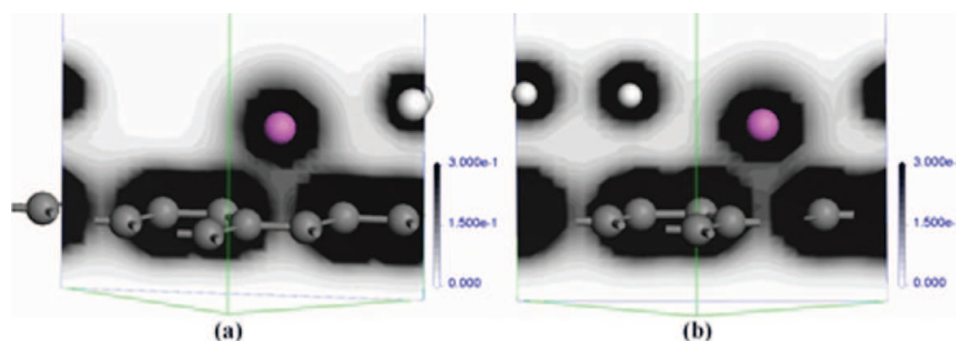


Fig. 25. Electron density distribution in the systems of one and two H₂ molecules adsorbed on graphene with Al adsorbed on a single side of graphene. (Reproduced with permission from Ref. (Ao & Peeters, 2010b). Copyright 2010, APS)

layer. In addition, some electronic distribution also appears among the H₂ molecules, the Al atom and the graphene layer. For H₂ molecules adsorbed on pristine graphene, no electron density was found between the H₂ molecules and the graphene layer (Ao et al., 2009a). Therefore, H₂ adsorption is enhanced in the Al-adsorbed graphene system due to the adsorbed Al atoms that act as bridges to link the electron clouds of the H₂ molecules and the graphene layer. Furthermore, Fig. 25(b) also shows that there is some electron distribution between the two adsorbed H₂ molecules. This means that the interaction between the H₂ molecules will change the electron distribution and may induce an enhancement of the adsorption energy as found in Fig. 24.

Very recently, the mechanism of H₂ adsorption onto Ca cation centers was investigated using both DFT and wave function approaches (Cha et al., 2009). It was found that DFT calculations overestimated the binding energy between the H₂ molecules and the Ca¹⁺ cation centers significantly. Similarly, a calculation was carried out on 2 H₂ molecules adsorbed on an Al coated graphene using the cluster model with both LDA and wave function approaches with MP2 within the Gaussian modules. The average binding energies for H₂ in this cluster system were found to be -0.196 and -0.185 eV/H₂ with LDA and MP2, respectively. Thus the two values differ by less than 6% giving some credibility to our numerical obtained binding energy.

In other words, the significant overestimation by DFT as found earlier for the binding of H₂ molecules onto Ca¹⁺ system does not occur for our system.

In addition, in order to investigate the effect of the simulation cell size on the results calculations were also performed using a 4 × 4 supercell with H₂ molecules adsorbed as shown in Fig. 23(a). We found almost the same results as obtained with the 2 × 2 supercell. In the 4 × 4 system, the H₂ molecules are adsorbed on the center sites of the equilateral triangles of Al atoms, as shown in Fig. 23(a). The distance between the H₂ molecules and the graphene surface are, respectively, 2.884 and 2.825 Å in 2 × 2 and 4 × 4 systems, while E_{b-H_2} in 4 × 4 system is -0.190 eV/H₂ and $E_{b-H_2} = -0.182$ eV/H₂ in 2 × 2 system.

For the case of hydrogen adsorption on Al that is adsorbed on both sides of graphene, the situations of one, two and three H₂ molecules adsorbed on each side of graphene are rather similar to the above case of adsorption on a single side of graphene. In other words, two H₂ molecules will take the center sites of equilateral triangles formed by the adsorbed Al atoms as shown in Figs. 23(a) and 23(b), and the third H₂ will take the top site of the Al atom as in Fig. 23(c). Previously, it is shown that a maximum of three H₂ molecules per 2 × 2 unit cell can be adsorbed on one side of graphene. However, for the case of adsorption on both sides of the graphene layer, each side can absorb more than 3 H₂ molecules. In Fig. 23(d) with 4 H₂ molecules adsorbed on each side, we show a 4 × 4 supercell. Two of them take the centre sites of equilateral triangles, and the other two are located on the bridge sites of two Al atoms. However, the four H₂ molecules are in two different planes with distances to the graphene layer being 2.672 and 4.675 Å. The distances of the four H₂ molecules to the Al atom are respectively 2.444, 2.531, 2.918, and 2.947 Å. The average E_{b-H_2} is -0.209 eV/H₂. If further increasing the number of H₂ molecules, the two H₂ molecules in the center sites of the equilateral triangles will hop to the bridge sites of the two Al atoms while keeping the two-layer structure. Therefore, each Al atom can absorb a maximum of six H₂ molecules, due to the two-layer adsorption structure and each Al atom has six nearest Al atoms with each adsorbed H₂ molecule shared by two Al atoms.

Fig. 23(e) gives the corresponding atomic structure with H₂ molecules fully adsorbed. It shows that all the H₂ molecules are located at the bridge sites of Al-Al and are arranged into two layers on each side of graphene. Note that the adsorption of H₂ on both sides of graphene will automatically change the sites of adsorbed Al atoms from the centre site of the carbon hexagon to nearly the bridge site of the C-C bond as shown in Figs. 23(d) and 23(e). The different location of the Al atoms in the presence of adsorbed H₂ for single side and both sides of graphene is a consequence of: (1) the different charges of Al atoms adsorbed on one side of graphene and on both sides of graphene, and (2) the different number of adsorbed H₂ molecules. Therefore, HSC is up to 13.79 wt% with an average $E_{b-H_2} = -0.193$ eV/H₂. Note that the obtained HSC is in excess of 6 wt%, surpassing DOE's target, and the obtained E_{b-H_2} is almost within the required range of -0.2 to -0.4 eV/H₂ (Li et al., 2003).

For the practical purpose, E_{b-H_2} is required to be a weak function of the adsorption coverage X of H₂ molecules on graphene, so that the adsorbed H₂ molecules can be desorbed to almost zero X . In this work, E_{b-H_2} is about -0.2 eV/H₂ and it is found that the amount of coverage has only a weak effect on E_{b-H_2} . The coverage dependence of $E_{b-H_2}(X)$ is shown in Fig. 26 with $E_{b-H_2}(X)$ varying within 15%. Note that E_{b-H_2} is the lowest when 4 H₂ molecules were adsorbed. This is because adsorption is strongest when H₂ molecules are located on the centre sites of equilateral triangles formed by the adsorbed Al atoms. This was confirmed above in Fig. 23(a) where one H₂ molecule was first adsorbed at the centre sites of the equilateral triangles. Due to the interaction between the H₂ molecules as shown in the Figs. 24, 25 and

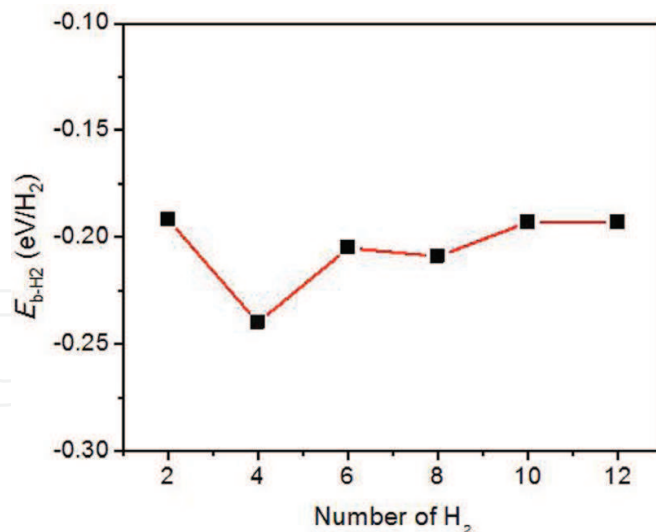


Fig. 26. X dependent average adsorption energy $E_{b-H_2}(X)$ of H_2 on graphene with Al adsorbed on both sides of graphene. (Reproduced with permission from Ref. (Ao & Peeters, 2010b). Copyright 2010, APS)

discussed above, adsorption with 2 H_2 molecules on each side on the centre sites of equilateral triangles is strongest.

When 12 H_2 molecules are adsorbed on both sides of a 2×2 supercell of graphene, the H_2 molecules on each side of graphene will be arranged into two layers as shown in Fig. 23(e), the distances of each layer to the graphene surface are respectively about 2.5 and 5.0 Å, while d_1 is about 2.2 Å. As discussed above, the adsorption energy E_{b-Al} for adsorption on both sides of graphene is larger than that for single side adsorption. At the same time, the Al atoms are more positively charged, and the C atoms are more negatively charged when the Al atoms are adsorbed on both sides of graphene. As found previously hydrogen adsorption is mainly induced by charged metal atoms, and the strength of the adsorption depends on the amount of the transferred charge (Liu et al., 2009; Sun et al., 2006). Thus, the graphene layer when Al is adsorbed on both sides of graphene has a larger capacity for H_2 storage. However, due to the limited space between the Al atoms and the repulsive interaction between the adsorbed H_2 molecules, some adsorbed H_2 molecules move upwards, over the Al atoms. This is also the reason why H_2 molecules can form a two-layer arrangement in the case of Al adsorbed on both sides of graphene, only a single H_2 layer is found for the corresponding single side system.

To test the stability of the hydrogen storage system, *ab initio* MD simulations was performed on a $12H_2$ -Al-graphene system which is shown in Fig. 23(e). The MD simulation in the NVT ensemble, i.e., constant number of atoms N , volume V , and temperature T , was performed over a time of 1 ps with a massive GGM thermostat at 300 K and without external pressure. We found that only the outer 2 H_2 molecules are escaping from each side of the graphene layer, because they are more weakly bound than the other H_2 molecules. For example, the first H_2 molecule that is released has a binding energy of -0.129 eV. In this case, the HSC becomes 9.64 wt%, which is still much higher than DOE's target. While *ab initio* MD simulation is quite computationally time consumption, 1 ps is not enough to get statistically meaningful values for the desorption temperature. However, it does suggest that the system keeps a rather high hydrogen storage capacity at room temperature. This is even the case in the absence of external pressure, and it is thus possible to release H_2 molecules without removing the Al atoms. Note

that the system stability of hydrogen storage in Ti-decorated carbon nanotubes was tested in similar conditions, where the MD calculations lasted 1.5 ps (Yildirim & Ciraci, 2005). In addition, the release of H₂ molecules can be further prevented by decreasing the temperature or increasing the pressure of storage to increase its HSC.

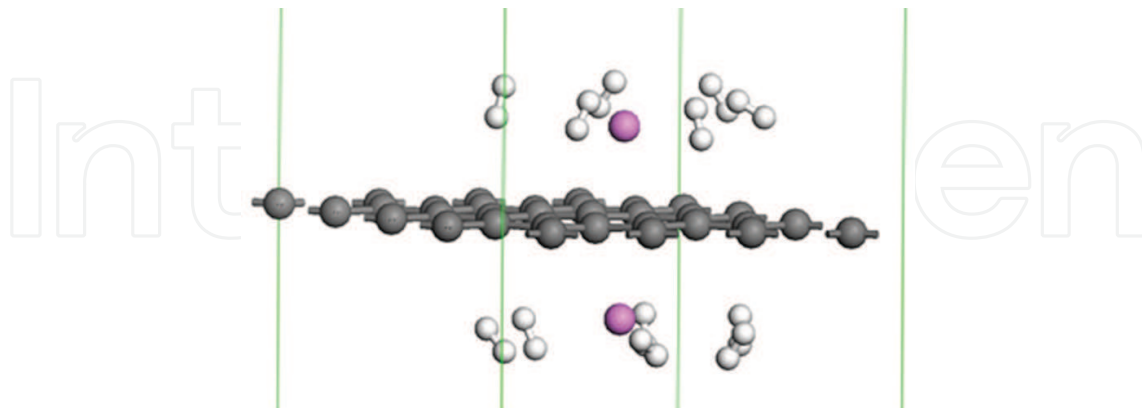


Fig. 27. The configuration of H₂ molecules adsorbed in a 4 supercell system. (Reproduced with permission from Ref. (Ao & Peeters, 2010b). Copyright 2010, APS)

To investigate the effect of the concentration of adsorbed Al atoms on its hydrogen storage capacity, a 4 × 4 graphene supercell was considered with one Al atom on the centre site of the carbon hexagon above and below the graphene layer. It is found that each Al atom can maximally adsorb 6 H₂ molecules with average $E_{b-H_2} = -0.172$ eV/H₂ resulting in a HSC of 5.19 wt%. The adsorption configuration is shown in Fig. 27. Note that the HSC is much lower than 13.79 wt% found for the 2 × 2 supercell system above. In the case of H₂ adsorbed in the 2 × 2 system, the H₂ molecules are adsorbed on the bridge sites of Al-Al and are arranged into a two layer configuration. Thus, each adsorbed H₂ molecule interacts with the nearest two Al atoms. In the 4 × 4 system, which corresponds to a lower density of adsorbed Al, the distance between two Al atoms is very long, up to 9.84 Å. Thus, each H₂ interacts with one Al atom and the graphene layer, and there is more space available for the adsorbed H₂ molecules which are located in a single layer. The corresponding adsorption energies E_{b-H_2} also decrease slightly as the Al-Al distance increases. For single H₂ molecule and two H₂ molecules adsorbed on a 4 × 4 supercell, E_{b-H_2} are -0.169 and -0.178 eV/H₂. In case of a 2 × 2 supercell we found that E_{b-H_2} are -0.182 and -0.227 eV/H₂, respectively.

For the practical applications, it is desirable to know the exact charge status of the hydrogen storage material. From it the information whether the hydrogen storage material is fully charged or the adsorbed H₂ molecules are completely released can be obtained. The charge exchanged with the graphene layer can be determined by the conductivity of the graphene layer, which is strongly determined by the DOS at the Fermi level (He et al., 2008; Schedin et al., 2007). The X-dependence of the latter quantity is given in Fig. 28. The result shows that the DOS at the Fermi level decreases as X increases and this dependence becomes weaker at high X.

4. Conclusion

A principle of CO adsorption enhancement was developed theoretically by using density functional theory through doping Al into graphene. The results show that the Al doped graphene has strong chemisorption of CO molecule by forming Al-CO bond, where CO onto intrinsic graphene remains weak physisorption. Furthermore, the enhancement of

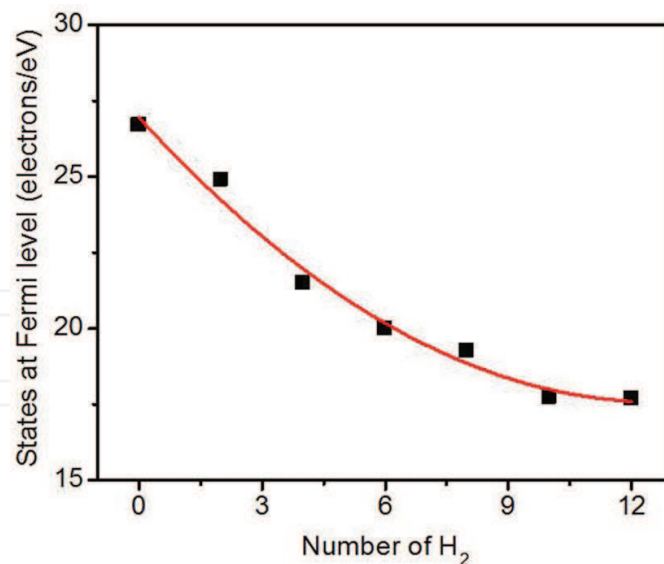


Fig. 28. X dependent number of band states at the Fermi level. (Reproduced with permission from Ref. (Ao & Peeters, 2010b). Copyright 2010, APS)

CO sensitivity in the Al doped graphene is determined by a large electrical conductivity change after adsorption, where CO absorption leads to increase of electrical conductivity via introducing large amount of shallow acceptor states. Therefore, this newly developed Al doped graphene would be an excellent candidate for sensing CO gas. After that, the correlation of the applied electric field F and adsorption/desorption behaviors of CO molecule in the Al doped graphene was studied. The results indicate that the positive F reduces the adsorption energies E_b of the CO adsorbed onto the doped graphene, while E_b increases under the negative F . Furthermore, desorption commences when a large positive F ($F \geq 0.03$ au) is applied. Finally, the thermal stability of interaction between the CO molecules and the Al doped graphene is studied with *ab initio* molecular dynamics calculation to reveal the adsorption/desorption behaviours of the system. Based on the results of the calculations, the adsorption/desorption phase diagram was established by the atomic thermodynamics and the temperature dependent desorption time $\tau(T)$ was determined with thermal desorption method. The results show that the optimal desorption temperature is 400 K. Meanwhile, the effect of T on atomic structure parameters and electrical properties were analyzed, and the results show that the greatest conductivity change before and after adsorption is at $T = 400$ K. Therefore, this sensor material has the best sensing performance with appropriate τ and the biggest conductivity change at 400 K.

Furthermore, the promising hydrogen storage mediums, Al-modified graphenes, are proposed through density functional theory calculations. Hydrogen molecule is predicted to be strongly physically adsorbed on Al substitutionally doped graphene with adsorption energy -0.427 eV/ H_2 that is in a reasonable range, so that hydrogen storage can be recycled at near ambient conditions, while a graphene layer with Al adsorbed on both sides can store hydrogen up to 13.79 wt% with a two-layer arrangement of H_2 molecules formed on each side. Its hydrogen storage capacity is in much excess of 6 wt% of DOE's target. In the Al substitutionally doped graphene system, it is believed that the doped Al alters the electronic structures of both C and H_2 , and the bands of H_2 overlapping with those of Al and C simultaneously are the underlying mechanism of the hydrogen adsorption enhancement from -0.159 eV/ H_2 in pristine graphene. In the Al adsorbed on both sides of graphene system, this

high-capacity hydrogen storage is due to the adsorbed Al atoms that act as bridges to link the electron clouds of the H₂ molecules and the graphene layer. In addition, we find that the H₂ concentration in the hydrogen storage medium can be measured by the change in the conductivity of the graphene layer.

There has been an explosion of ideas that suggest graphene for potential applications. This is often led by analogies with carbon nanotubes that continue to serve as a guide in searching for new applications. Except for its excellent electronic properties, graphene also displays several unusual attributions. Graphene is a giant aromatic macromolecule that conducts both electricity and heat well in two dimensions. Their mechanical strength of graphene is comparable to that of CNTs, while CNTs can be considered as a rolled up graphene. The shape, size, and chemical structure of graphene sheets can be further modified by engineering. Nonetheless, research toward the application of graphene-based materials has just begun. Many challenges and opportunities remain. For examples, applications for batteries and supercapacitors, in separation technologies, as supports for catalysts, and filler for composition materials, and so on, are widely expected in the recent future.

5. Acknowledgement

This work was financially supported by the Vice-Chancellor's postdoctoral research fellowship program of the University of New South Wales (SIR50/PS19184) and the Australian Research Council Discovery Programs (DP1096769 and DP0988687).

6. References

- Acharya, C. & Turner, C. (2007). Effect of an electric field on the adsorption of metal clusters on boron-doped carbon surfaces, *J. Phys. Chem. C* 111: 14804–14812.
- Ao, Z., Jiang, Q., Zhang, R., Tan, T. & Li, S. (2009a). Al doped graphene: A promising material for hydrogen storage at room temperature, *J. Appl. Phys.* 105: 074307–074312.
- Ao, Z., Li, S. & Jiang, Q. (2009b). Thermal stability of interaction between the CO molecules and the Al doped graphene, *Phys. Chem. Chem. Phys.* 11: 1683–1687.
- Ao, Z., Li, S. & Jiang, Q. (2010a). Correlation of the applied electrical field and CO adsorption/desorption behavior on Al-doped graphene, *Solid State Commun.* 150: 680–683.
- Ao, Z. & Peeters, F. (2010b). High-capacity hydrogen storage in Al-adsorbed graphene, *Phys. Rev. B* 81: 205406–205412.
- Ao, Z., Yang, J., Li, S. & Jiang, Q. (2008). Enhancement of CO detection in Al doped graphene, *Chem. Phys. Lett.* 461: 276–279.
- Arellano, J., Molina, L., Rubio, A. & Alonso, J. (2000). Density functional study of molecular hydrogen on graphene layers, *J. Chem. Phys.* 112: 8114–8119.
- Ataca, C., Aktürk, E. & Ciraci, S. (2009). Hydrogen storage of calcium atoms adsorbed on graphene: First-principle plane wave calculations, *Phys. Rev. B* 79: 041406–041409.
- Beenakker, C. (2008). Colloquium: Andreev reflection and Klein tunneling in graphene, *Rev. Mod. Phys.* 80: 1337–1354.
- Blyholder, G. (1964). Molecular orbital view of chemisorbed carbon monoxide, *J. Phys. Chem.* 68: 2772–2777.

- Bunch, J., Yaish, Y., Brink, M., Bolotin, K. & McEuen, P. (2005). Coulomb oscillations and hall effect in quasi-2D graphite quantum dots, *Nano Lett.* 5: 287–290.
- Cabria, I., López, M. & Alonso, J. (2008). Hydrogen storage in pure and Li-doped carbon nanopores: Combined effects of concavity and doping, *J. Chem. Phys.* 128: 144704–144711.
- Ceperley, D. & Alder, B. (1980). Ground state of the electron gas by a stochastic method, *Phys. Rev. Lett.* 45: 566–569.
- Cha, J., Lim, S., C.H., C., Cha, M.-H. & Park, N. (2009). Inaccuracy of density functional theory calculations for dihydrogen binding energetic onto Ca cation centers, *Phys. Rev. Lett.* 103: 216102–216105.
- Chandrakumar, K. & Ghosh, S. (2008). Alkali-metal-induced enhancement of hydrogen adsorption in C₆₀ fullerene: An ab initio study, *Nano Lett.* 8: 13–19.
- Collins, P., Bradley, K., Ishigami, M. & Zettl, A. (2000). Extreme oxygen sensitivity of electronic properties of carbon nanotubes, *Science* 287: 1801–1804.
- Coontz, R. & Hanson, B. (2004). Not so simple, *Science* 305: 957.
- Degall, M., Lindan, P., Probert, M., Pickard, C., Hasnip, P., Clark, S. & Payne, M. (2002). First-principles simulation: ideals, illustrations and the CASTEP code, *J. Phys.: Condens. Matter* 14: 2717–2744.
- Delley, B. (1990). An all-electron numerical method for solving the local density functional for polyatomic molecules, *J. Chem. Phys.* 92: 508–517.
- Delley, B. (2000). From molecules to solids with the DMol³ approach, *J. Chem. Phys.* 113: 7756–7764.
- Delley, B. (2002). Hardness conserving semilocal pseudopotentials, *Phys. Rev. B* 66: 155125.
- Deng, W., Xu, X. & Goddard, W. (2004). New alkali doped pillared carbon materials designed to achieve practical reversible hydrogen storage for transportation, *Phys. Rev. Lett.* 92: 166103–166106.
- Durgun, E., Ciraci, S., Zhou, W. & Yildirim, T. (2006). Transition-metal-ethylene complexes as high-capacity hydrogen-storage media, *Phys. Rev. Lett.* 97: 226102–226105.
- Froudakis, G. (2001). Why alkali-metal-doped carbon nanotubes possess high hydrogen uptake, *Nano Lett.* 1: 531–533.
- Gao, G., Gagin, T. & Goddard, I. W. (1998). Inaccuracy of density functional theory calculations for dihydrogen binding energetic onto Ca cation centers, *Phys. Rev. Lett.* 80: 5556–5559.
- Gaudoin, R., Foulkes, W. & Rajagopal, G. (2002). Ab initio calculations of the cohesive energy and the bulk modulus of aluminium, *J. Phys.: Condens. Matter* 14: 8787–8793.
- Geim, A. & Novoselov, K. (2007). The rise of graphene, *Nat. Mater.* 6: 183–191.
- Ghosh, A., Subrahmanyam, K., Krishna, K., Datta, S., Govindaraj, A., Pati, S. & Rao, C. (2008). Uptake of H₂ and CO₂ by graphene, *J. Phys.Chem. C* 112: 15704–15707.
- Girifacol, L. & Hodak, M. (2002). Van der waales binding energies in graphitic structures, *Phys. Rev. B* 65: 125404–125408.
- Graetz, J., Chaudhuri, S., Lee, Y., Vogt, T., Muckerman, J. & Reilly, J. (2006). Pressure-induced structural and electronic changes in α -AlH₃, *Phys. Rev. B* 74: 214114–214120.

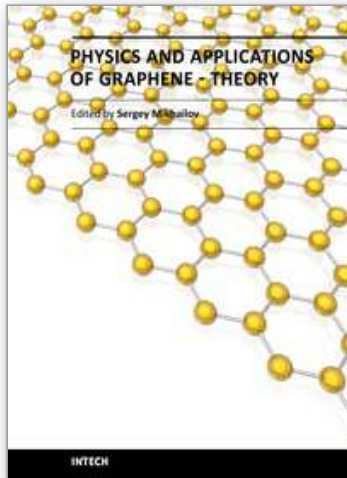
- Hammer, B., Hansen, L. & Nørskov, J. (1999). Improved adsorption energetics within density-functional theory using revised perdue-burke-ernzerhof functionals, *Phys. Rev. B* 59: 7413–7421.
- He, C., Zhang, P., Zhu, Y. & Jiang, Q. (2008). Structures and quantum conduction of copper nanowires under electric field using first principles, *J. Phys. Chem. C* 112: 9045–9049.
- Hyman, M. & Medlin, J. (2005). Theoretical study of the adsorption and dissociation of oxygen on Pt(111) in the presence of homogeneous electric fields, *J. Phys. Chem. B* 109: 6304–6310.
- Jeloaica, L. & Sidis, V. (1999). DFT investigation of the adsorption of atomic hydrogen on a cluster-model graphite surface, *Chem. Phys. Lett.* 300: 157–162.
- Klontzas, E., Mavrandonakis, A., Tylianakis, E. & Froudakis, G. (2008). Improving hydrogen storage capacity of MOF by functionalization of the organic linker with lithium atoms, *Nano Lett.* 8: 1572–1576.
- Kong, J., Chapline, M. & Dai, H. (2001). Functionalized carbon nanotubes for molecular hydrogen sensors, *Adv. Mater.* 13: 1384–1386.
- Kong, J., Franklin, N., Zhou, C., Chapline, M., Peng, S., Cho, K. & Dai, H. (2000). Nanotube molecular wires as chemical sensors, *Science* 287: 622–625.
- Koper, M. & van Santen, R. (1999). Electric field effects on CO and NO adsorption at the Pt(111) surface, *J. Electroanal. Chem.* 476: 64–70.
- Krasnov, P., Ding, F., Singh, A. & Yakobson, B. (2007). Clustering of Sc on SWNT and reduction of hydrogen uptake: Ab-initio all electron calculations, *J. Phys. Chem. C* 111: 17977–17980.
- Lee, C., Wei, X., Kysar, J. & Hone, J. (2008). Measurement of the elastic properties and intrinsic strength of monolayer graphene, *Science* 321: 385–388.
- Leenaerts, O., Partoens, B. & Peeters, F. (2008). Adsorption of H₂O, NH₃, CO, NO₂, and NO on graphene: A first-principles study, *Phys. Rev. B* 77: 125416–125422.
- Li, D., Müller, M., Gilje, S. & Kaner, R. (2008a). Processable aqueous dispersions of graphene nanosheets, *Nat. Nanotechnol.* 3: 101–105.
- Li, J., Furuta, T., Goto, H., Ohashi, T., Fujiwara, Y. & Yip, S. (2003). Theoretical evaluation of hydrogen storage capacity in pure carbon nanostructures, *J. Chem. Phys.* 119: 2376–2385.
- Li, X., Grubisic, A., Stokes, S., Cordes, J., Ganteför, G., Bowen, K., Kiran, B., Willis, M., Burgert, P. & Schnöckel, H. (2007). Unexpected stability of Al₄H₆: A borane analog?, *Science* 315: 356–358.
- Li, X., Wang, X., Zhang, L., Lee, S. & Dai, H. (2008b). Chemically derived, ultrasoft graphene nanoribbon semiconductors, *Science* 319: 1229.
- Lide, D. (2000). *CRC Handbook of Chemistry and Physics*, CRC Press, Boca Raton, FL.
- Liu, W., Zhao, Y., Li, Y., Jiang, Q. & Lavernia, E. (2009). Enhanced hydrogen storage on Li-dispersed carbon nanotubes, *J. Phys. Chem. C* 113: 2028–2033.
- Loffreda, D. (2006). Theoretical insight of adsorption thermodynamics of multifunctional molecules on metal surfaces, *Surf. Sci.* 600: 2103–2112.
- Lozovoi, A. & Alavi, A. (2007). Vibrational frequencies of CO on Pt(111) in electric field: A periodic DFT study, *J. Electroanal. Chem.* 607: 140–146.

- Lugo-Solis, A. & Vasiliev, I. (2007). Ab initio study of K adsorption on graphene and carbon nanotubes: Role of long-range ionic forces., *Phys. Rev. B* 76: 235431–235438.
- Mares, A. & Van Ruitenbeek, J. (2005). Observation of shell effects in nanowires for the noble metals Cu, Ag, and Au, *Phys. Rev. B* 72: 205402–205408.
- McEwen, J.-S., Gaspard, P., Mittendorfer, F., Visart de Bocarmé, T. & Kruse, N. (2008). Field-assisted oxidation of rhodium, *Chem. Phys. Lett.* 452: 133–138.
- Moseley, P. (1997). Solid state gas sensors, *Meas. Sci. Technol.* 8: 223–227.
- Mpourmpakis, G., Tylianakis, E. & Froudakis, G. (2007). Carbon nanoscrolls: A promising material for hydrogen storage, *Nano Lett.* 7: 1893–1897.
- Nikitin, A., Li, X., Zhang, Z., Ogasawara, H., Dai, H. & Nilsson, A. (2008). Hydrogen storage in carbon nanotubes through the formation of stable C-H bonds, *Nano Lett.* 8: 162–167.
- Nose, S. (1984). A molecular dynamics method for simulations in the canonical ensemble, *Mol. Phys.* 52: 255–268.
- Nose, S. (1991). Constant temperature molecular dynamics methods, *Prog. Theor. Phys. Supplement* 103: 1–46.
- Novoselov, K., A.K., G., Morozov, S., Jiang, D., Zhang, Y., Dubonos, S., Grigorieva, I. & Firsov, A. (2004). Electric field effect in atomically thin carbon films, *Science* 306: 666–669.
- Okamoto, Y. & Miyamoto, Y. (2001). Ab initio investigation of physisorption of molecular hydrogen on planar and curved graphenes, *J. Phys. Chem. B* 105: 3470–3474.
- Panella, B., Hirscher, M. & Roth, S. (2005). Hydrogen adsorption in different carbon nanostructures, *Carbon* 43: 2209–2214.
- Parrinello, M. & Rahman, A. (1981). Polymorphic transitions in single crystals: A new molecular dynamics method., *J. Appl. Phys.* 52: 7182–7190.
- Peng, S. & Cho, K. (2003). Ab initio study of doped carbon nanotubes sensors, *Nano Lett.* 3: 513–517.
- Peng, S., Cho, K., Qi, P. & Dai, H. (2004). Ab initio study of CNT NO₂ gas sensor, *Chem. Phys. Lett.* 387: 271–276.
- Perdew, J. & Zunger, A. (1981). Self-interaction correction to density-functional approximations for many-electrons systems, *Phys. Rev. B* 23: 5048–5079.
- Peres, N., Guinea, F. & Castro Neto, A. (2006). Electronic properties of disordered two-dimensional carbon, *Phys. Rev. B* 73: 125411.
- Peres, N., Klironomos, F., Tsai, S.-W., Santos, J., Lopes dos Santos, J. & Castro Neto, A. (2007). Electron waves in chemically substituted graphene, *Euro. Phys. Lett.* 87: 67007.
- Peres, N., Tsai, S.-W., Santos, J. & Ribeiro, R. (2009). Scanning tunneling microscopy currents on locally disordered graphene, *Phys. Rev. B* 7879: 155442.
- Raaen, S. & Ramstad, A. (2005). Monte-Carlo simulations of thermal desorption of adsorbed molecules from metal surface, *Energy* 30: 821–830.
- Rao, C., Sood, A., Subrahmanyam, K. & Govindaraj, A. (2009). Graphene: The new two-dimensional nanomaterial, *Angew. Chem. Int. Ed.* 48: 7752–7778.
- Readhead, P. (1962). Thermal desorption of gases, *Vacuum* 12: 203–211.
- Reina, A., Jia, X., Ho, J., Nezich, D., Son, H., Bulovic, V., Dresselhaus, M. & Kong, J. (2009). Large area, few-layer graphene films on arbitrary substrates by chemical vapor deposition, *Nano Lett.* 9: 30–35.

- Sahaym, U. & Norton, M. (2008). Advances in the application of nanotechnology in enabling a hydrogen economy, *J. Mater. Sci.* 43: 5395–5429.
- Schedin, F., G. A., Morozov, S., Hill, E., Blake, P., Katasnelson, M. & Novoselov, K. (2007). Detection of individual gas molecules adsorbed on graphene, *Nat. Mater.* 6: 652–655.
- Schlapbach, L. & Züttel, A. (2001). Hydrogen-storage materials for mobile applications, *Nature* 414: 353–358.
- Seitsonen, A., Kim, Y., Knapp, M., Wendt, S. & Over, H. (2001). CO adsorption on the reduced RuO₂(110) surface: Energetics and structure, *Phys. Rev. B* 65: 035413–035421.
- Spencer, M. & Yarovsky, I. (2007). Ab initio molecular dynamics study of H₂S dissociation on the Fe(110) surface, *J. Phys. Chem. C* 111: 16372–16378.
- Sun, Q., Jena, P., Wang, Q. & Marquez, M. (2006). First-principles study of hydrogen storage on Li₁₂C₆₀, *J. Am. Chem. Soc.* 128: 9741–9745.
- Suzuki, M. (1991). General theory of fractal path integrals with applications to many-body theories and statistical physics, *J. Math. Physics* 32: 400–407.
- Tada, K., Furuya, S. & Watanabe, K. (2001). Ab initio study of hydrogen adsorption to single-walled carbon nanotubes, *Phys. Rev. B* 63: 155405–155408.
- Tielens, F., Gracia, L., Polo, V. & Andrés, J. (2007). A theoretical study on the electronic structure of Au-XO^(0,-1,+1) (X=C, N, and O) complexes: effect of an external electric field, *J. Phys. Chem. A* 111: 13255–13263.
- Todorova, N., Spencer, M. & Yarovsky, I. (2007). Ab initio study of s dynamics on iron surface, *Surf. Sci.* 601: 665–671.
- Tomanek, D., Kreuzer, H. & Block, J. (1985). Tight-binding approach to field desorption: N₂ on Fe(111), *Surf. Sci.* 157: L315–322.
- Tosatti, E., Prestipino, S., Kostlmeier, S., Dal Corso, A. & Di Tolla, F. (2001). String tension and stability of magic tip-suspended nanowires, *Science* 291: 288–290.
- Verlet, L. (1967). Computer experiments on classical fluids. I. thermodynamical properties of Lennard-Jones molecules, *Phys. Rev.* 159: 98–103.
- Wang, R., Zhang, D., Sun, W., Han, Z. & Liu, C. (2007). A novel aluminum-doped carbon nanotubes sensor for carbon monoxide, *J. Molecular Struc.: Theochem.* 806: 93–97.
- Wehling, T.O., N. K., Morozov, S., Vdovin, E., Katsnelson, M., Geim, A. & Lichtenstein, A. (2008). Molecular doping of graphene, *Nano Lett.* 8: 173–175.
- Wei, B., Hsu, M., Su, P., Lin, H., Wu, R. & Lai, H. (2004). A novel SnO₂ gas sensor doped with carbon nanotubes operating at room temperature., *Sensor Actuat.* 101: 81–89.
- Wei, D., Liu, Y., Wang, Y., Zhang, H., Huang, L. & Yu, G. (2009). Synthesis of N-doped graphene by chemical vapor deposition and its electrical properties, *Nano Lett.* 9: 1752–1758.
- Wu, G., Zhang, J., Wu, Y., Li, Q., Chou, K. & Bao, X. (2009). Adsorption and dissociation of hydrogen on MgO surface: A first-principles study, *J. Alloy Compd.* 480: 788–793.
- Xu, W., Takahashi, K., Matsuo, Y., Hattori, Y., Kumagai, M., Ishiyama, S., Kaneko, K. & Iijima, S. (2007). Investigation of hydrogen storage capacity of various carbon materials, *Int. J. Hydrogen Energy* 32: 2504–2512.
- Yang, W., Rantinac, K., Ringer, S., Thordarson, P., Gooding, J. & Braet, F. (2010). Carbon nanomaterials in biosensors: Should you use nanotubes or graphene?, *Angew. Chem. Int. Ed.* 49: 2114–2138.

- Ye, Y., Ahn, C., Witham, C., Fultz, B., Liu, J., Rinzler, A., Colbert, D., Smith, K. & Smalley, R. (1999). Hydrogen adsorption and cohesive energy of single-walled carbon nanotubes, *Appl. Phys. Lett.* 74: 2307–2309.
- Yildirim, T. & Ciraci, S. (2005). Titanium-decorated carbon nanotubes as a potential high capacity hydrogen storage medium, *Phys. Rev. Lett.* 94: 177501–177504.
- Yoon, M., Yang, S., Hicke, C., Wang, E. & Zhang, Z. (2008). Calcium as the superior coating metal in functionalization of carbon fullerenes for high-capacity hydrogen storage., *Phys. Rev. Lett.* 100: 206806–206809.
- Yoshida, H. (1990). Construction of higher order symplectic integrators, *Phys. Lett. A* 150: 262–268.
- Yuan, G., Zhang, W., Yang, Y., Tang, Y., Li, Y., Wang, J., Meng, X., He, Z., Wu, C., Bello, I., Lee, C. & Lee, S. (2009). Graphene sheets via microwave chemical vapor deposition, *Chem. Phys. Lett.* 467: 361–364.
- Zhang, Y., Tan, Y. & Stormer, H. (2005). Experimental observation of the quantum hall effect and berry's phase in graphene, *Nature* 438: 201–204.
- Zhang, Y., Zhang, D. & Liu, C. (2006). Novel chemical sensor for cyanides: Boron-doped carbon nanotubes, *J. Phys. Chem. B* 110: 4671–4674.
- Zhao, Q., Nardelli, M., Lu, W. & Bernholc, J. (2005). Carbon nanotube-metal cluster composites: A new road to chemical sensors?, *Nano Lett.* 5: 847–851.
- Zhou, S., Gweon, G.-H., Fedorov, A., First, P., de Heer, W., Lee, D.-H., Guinea, F., Castro, A. & Lanzara, A. (2007). Substrate-induced bandgap opening in epitaxial graphene, *Nat. Mater.* 6: 770–775.

IntechOpen



Physics and Applications of Graphene - Theory

Edited by Dr. Sergey Mikhailov

ISBN 978-953-307-152-7

Hard cover, 534 pages

Publisher InTech

Published online 22, March, 2011

Published in print edition March, 2011

The Stone Age, the Bronze Age, the Iron Age... Every global epoch in the history of the mankind is characterized by materials used in it. In 2004 a new era in material science was opened: the era of graphene or, more generally, of two-dimensional materials. Graphene is the strongest and the most stretchable known material, it has the record thermal conductivity and the very high mobility of charge carriers. It demonstrates many interesting fundamental physical effects and promises a lot of applications, among which are conductive ink, terahertz transistors, ultrafast photodetectors and bendable touch screens. In 2010 Andre Geim and Konstantin Novoselov were awarded the Nobel Prize in Physics "for groundbreaking experiments regarding the two-dimensional material graphene". The two volumes *Physics and Applications of Graphene - Experiments* and *Physics and Applications of Graphene - Theory* contain a collection of research articles reporting on different aspects of experimental and theoretical studies of this new material.

How to reference

In order to correctly reference this scholarly work, feel free to copy and paste the following:

Zhimin Ao, Jack Yang and Sean Li (2011). Applications of Al Modified Graphene on Gas Sensors and Hydrogen Storage, *Physics and Applications of Graphene - Theory*, Dr. Sergey Mikhailov (Ed.), ISBN: 978-953-307-152-7, InTech, Available from: <http://www.intechopen.com/books/physics-and-applications-of-graphene-theory/applications-of-al-modified-graphene-on-gas-sensors-and-hydrogen-storage>

INTECH
open science | open minds

InTech Europe

University Campus STeP Ri
Slavka Krautzeka 83/A
51000 Rijeka, Croatia
Phone: +385 (51) 770 447
Fax: +385 (51) 686 166
www.intechopen.com

InTech China

Unit 405, Office Block, Hotel Equatorial Shanghai
No.65, Yan An Road (West), Shanghai, 200040, China
中国上海市延安西路65号上海国际贵都大饭店办公楼405单元
Phone: +86-21-62489820
Fax: +86-21-62489821

© 2011 The Author(s). Licensee IntechOpen. This chapter is distributed under the terms of the [Creative Commons Attribution-NonCommercial-ShareAlike-3.0 License](#), which permits use, distribution and reproduction for non-commercial purposes, provided the original is properly cited and derivative works building on this content are distributed under the same license.

IntechOpen

IntechOpen